Historical and future contributions of inland waters to the Congo basin carbon balance

Adam Hastie[1,2], Ronny Lauerwald[2,3,4], Philippe Ciais[3], Fabrice Papa[5,6], Pierre Regnier[2]

[1]School of GeoSciences, University of Edinburgh, EH9 3FF, Edinburgh, Scotland, UK
[2]Biogeochemistry and Earth System Modelling, Department of Geoscience, Environment and Society, Université Libre de Bruxelles, Bruxelles, 1050, Belgium
[3]Laboratoire des Sciences du Climat et de l'Environnement (LSCE), CEA CNRS UVSQ, Gif-sur-Yvette 91191, France
[4]Université Paris-Saclay, INRAE, AgroParisTech, UMR ECOSYS, 78850, Thiverval-Grignon, France
[5]Laboratoire d'Etudes en Géophysique et Océanographie Spatiales, Centre National de la Recherche Scientifique–Institut de recherche pour le développement–Université Toulouse Paul Sabatier–Centre national d'études spatiales, 31400 Toulouse, France
[6]Indo-French Cell for Water Sciences, International Joint Laboratory Institut de Recherche pour le Développement and Indian Institute of Science, Indian Institute of Science, 560012 Bangalore, India

Correspondence to: Adam Hastie (adam.hastie@ed.ac.uk)

Abstract

As the second largest area of contiguous tropical rainforest and second largest river basin in the world, the Congo basin has a significant role to play in the global carbon (C) cycle. For the present day, it has been shown that a significant proportion of global terrestrial net primary productivity (NPP) is transferred laterally to the land-ocean aquatic continuum (LOAC) as dissolved CO_2, dissolved organic carbon (DOC) and particulate organic carbon (POC). Whilst the importance of LOAC fluxes in the Congo basin has been demonstrated for the present day, it is not known to what extent these fluxes have been perturbed historically, how they are likely to change under future climate change and land use scenarios, and in turn what impact these changes might have on the overall C cycle of the basin. Here we apply the ORCHILEAK model to the Congo basin and estimate that 4% of terrestrial NPP (NPP = 5,800 ±166 Tg C yr^{-1}) is

currently exported from soils and vegetation to inland waters. Further, our results suggest that aquatic C fluxes may have undergone considerable perturbation since 1861 to the present day, with aquatic CO_2 evasion and C export to the coast increasing by 26% (186 ±41 Tg C yr^{-1} to 235 ±54 Tg C yr^{-1}) and 25% (12 ±3 Tg C yr^{-1} to 15 ±4 Tg C yr^{-1}) respectively, largely because of rising atmospheric CO_2 concentrations. Moreover, under climate scenario RCP 6.0 we predict that this perturbation could continue; over the full simulation period (1861-2099), we estimate that aquatic CO_2 evasion and C export to the coast could increase by 79% and 67% respectively. Finally, we show that the proportion of terrestrial NPP lost to the LOAC could increase from approximately 3% to 5% from 1861-2099 as a result of increasing atmospheric CO_2 concentrations and climate change. However, our future projections of the Congo basin C fluxes in particular need to be interpreted with some caution due to model limitations. We discuss these limitations, including the wider challenges associated with applying the current generation of land surface models which ignore nutrient dynamics to make future projections of the tropical C cycle, along with potential next steps.

1. Introduction

As the world's second largest area of contiguous tropical rainforest and second largest river, the Congo basin has a significant role to play in the global carbon (C) cycle. Current estimates of its C stocks and fluxes are limited by a sparsity of field data and therefore have substantial uncertainties, both quantified and unquantified (Williams et al., 2007; Lewis et al., 2009; Dargie et al., 2017). Nevertheless, it has been estimated that there is approximately 50 Pg C stored in its above ground biomass (Verhegghen et al., 2012), and up to 100 Pg C contained within its soils (Williams et al., 2007). Moreover, a recent study estimated that around 30 (6.3–46.8) Pg C is stored in the peats of the Congo alone (Dargie at al., 2017). Field data suggest that storage in tree biomass increased by 0.34 (0.15- 0.43) Pg C yr^{-1} in intact African tropical forests between 1968-2007 (Lewis et al., 2009) due in large part to a combination of increasing

atmospheric CO_2 concentrations and climate change (Ciais et al., 2009; Pan et al., 2015), while satellite data indicates that terrestrial net primary productivity (NPP) has increased by an average of 10 g C m^{-2} yr^{-1} per year between 2001 and 2013 in tropical Africa (Yin et al., 2017).

At the same time, forest degradation, clearing for rotational agriculture and logging are causing C losses to the atmosphere (Zhuravleva et al., 2013; Tyukavina et al., 2018) while droughts have reduced vegetation greenness and water storage over the last decade (Zhou et al., 2014). A recent estimate of above ground C stocks of tropical African forests, mainly in the Congo, indicates a minor net C loss from 2010 to 2017 (Fan et al., 2019). Moreover, recent field data suggests that the above ground C sink in tropical Africa was relatively stable from 1985 to 2015 (Hubau et al., 2020).

There are large uncertainties associated with projecting future trends in the Congo basin terrestrial C cycle, firstly related to predicting which trajectories of future CO_2 levels and land use changes will occur, and secondly to our ability to fully understand and simulate these changes and in turn their impacts. Future model projections for the 21st century agree that temperature will significantly increase under both low and high emission scenarios (Haensler et al., 2013), while precipitation is only projected to substantially increase under high emission scenarios, the basin mean remaining more or less unchanged under low emission scenarios (Haensler et al., 2013). Uncertainties in future land-use change projections for Africa are among the highest for any continent (Hurtt et al., 2011).

For the present day at the global scale, it has been estimated that between 1 and 5 Pg C yr^{-1} is transferred laterally to the land-ocean aquatic continuum (LOAC) as dissolved CO_2, dissolved organic carbon (DOC) and particulate organic carbon (POC) (Cole at al., 2007; Battin et al., 2009; Regnier et al., 2013; Drake et al., 2018; Ciais et al. 2020). This C can subsequently be evaded back to the atmosphere as CO_2, undergo sedimentation in wetlands and inland waters,

or be transported to estuaries or the coast. The tropical region is a hotspot area for inland water C cycling (Richey et al., 2002; Melack et al., 2004; Abril et al., 2014; Borges et al., 2015[a]; Lauerwald et al., 2015) due to high terrestrial NPP and precipitation, and a recent study used an upscaling approach based on observations to estimate present day CO_2 evasion from the rivers of the Congo basin at 251±46 Tg C yr^{-1} and the lateral C (TOC +DIC) export to the coast at 15.5 (13-18) Tg C yr^{-1} (Borges at al., 2015[a]; Borges et al., 2019). To put this into context, their estimate of aquatic CO_2 evasion represents 39% of the global value estimated by Lauerwald et al. (2015, 650 Tg C yr^{-1}) or 14% of the global estimate of Raymond et al. (2013, 1,800 Tg C yr^{-1}). Note that while Lauerwald et al. (2015) and Raymond et al. (2013) relied largely on the same database of partial pressure of CO_2 (pCO_2) measurements (GloRiCh, Hartmann et al., 2014) as the basis for their estimates, they took different, albeit both empirically led approaches. Moreover, both approaches were limited by a relative paucity of data from the tropics, which also explains the high degree of uncertainty associated with our understanding of global riverine CO_2 evasion.

Whilst the importance of LOAC fluxes in the Congo basin has been demonstrated for the present day, it is not known to what extent these fluxes have been perturbed historically, how they are likely to change under future climate change and land use scenarios, and in turn what impact these changes might have on the overall C balance of the Congo. In light of these knowledge gaps, we address the following research questions:

- What is the relative contribution of LOAC fluxes (CO_2 evasion and C export to the coast) to the present-day C balance of the basin?
- To what extent have LOAC fluxes changed from 1860 to the present day and what are the primary drivers of this change?

- How will these fluxes change under future climate and land use change scenarios (RCP 6.0 which represents the "no mitigation scenario") and what are the implications of this change?

Understanding and quantifying these long-term changes requires a complex and integrated mass-conservation modelling approach. The ORCHILEAK model (Lauerwald et al., 2017), a new version of the land surface model ORCHIDEE (Krinner et al., 2005), is capable of simulating observed terrestrial and aquatic C fluxes in a consistent manner for the present day in the Amazon (Lauerwald et al., 2017) and Lena (Bowring et al., 2019[a]; Bowring et al., 2019[b]) basins, albeit with limitations including a lack of explicit representation of POC fluxes and in-stream autotrophic production (see Lauerwald et al., 2017; Bowring et al., 2019[a]; Bowring et al., 2019[b] and Hastie et al., 2019 for further discussion). Moreover, it was recently demonstrated that this model could recreate observed seasonal and interannual variation in Amazon aquatic and terrestrial C fluxes (Hastie et al., 2019).

In order to accurately simulate aquatic C fluxes, it is crucial to provide a realistic representation of the hydrological dynamics of the Congo River, including its wetlands. Here, we develop new wetland forcing files for the ORCHILEAK model from the high-resolution dataset of Gumbricht et al. (2017) and apply the model to the Congo basin. After validating the model against observations of discharge, flooded area, DOC concentrations and pCO_2 for the present day, we then use the model to understand and quantify the long- term (1861-2099) temporal trends in both the terrestrial and aquatic C fluxes of the Congo Basin.

2. Methods

ORCHILEAK (Lauerwald et al., 2017) is a branch of the ORCHIDEE land surface model (LSM), building on past model developments such as ORCHIDEE-SOM (Camino Serrano, 2018), and represents one of the first LSM-based approaches which fully integrates the aquatic

C cycle within the terrestrial domain. ORCHILEAK simulates DOC production in the canopy and soils, the leaching of dissolved CO_2 and DOC to the river from the soil, the mineralization of DOC, and in turn the evasion of CO_2 to the atmosphere from the water surface. Moreover, it represents the transfer of C between litter, soils and water within floodplains and swamps (see section 2.2). Once within the river routing scheme, ORCHILEAK assumes that the lateral transfer of CO_2 and DOC are proportional to the volume of water. DOC is divided into a refractory and labile pool within the river, with half-lives of 80 and 2 days respectively. The refractory pool corresponds to the combined slow and passive DOC pools of the soil C scheme, and the labile pool corresponds to the active soil pool (see section 2.4.1). The concentration of dissolved CO_2 and the temperature-dependent solubility of CO_2 are used to calculate pCO_2 in the water column. In turn, CO_2 evasion is calculated based on pCO_2, along with a diurnally variable water surface area and a gas exchange velocity. Fixed gas exchange velocities of 3.5 m d^{-1} and 0.65 m d^{-1} respectively are used for rivers (including open floodplains) and forested floodplains.

In this study, as in previous studies (Lauerwald et al., 2017, Hastie et al. 2019, Bowring et al., 2019[a,b]), we run the model at a spatial resolution of 1° and use the default time step of 30 min for all vertical transfers of water, energy and C between vegetation, soil and the atmosphere, and the daily time-step for the lateral routing of water. Until now, in the Tropics, ORCHILEAK has been parameterized and calibrated only for the Amazon River basin (Lauerwald et al., 2017, Hastie et al. 2019). To adapt and apply ORCHILEAK to the specific characteristics of the Congo River basin (2.1), we had to establish new forcing files representing the maximal fraction of floodplains (MFF) and the maximal fraction of swamps (MFS) (2.2) and to recalibrate the river routing module of ORCHILEAK (2.3). All of the processes represented in ORCHILEAK remain identical to those previously represented for the Amazon ORCHILEAK (Lauerwald et al., 2017; Hastie et al., 2019). In the following methodology sections, we

describe; 2.1- Congo basin description, 2.2- Development of floodplains and swamps forcing files, 2.3- Calibration of hydrology, 2.4- Simulation set-up, 2.5- Evaluation and analysis of simulated fluvial C fluxes, and 2.6- Calculating the net carbon balance of the Congo Basin. For a full description of the ORCHILEAK model please see Lauerwald et al. (2017).

2.1 Congo basin description

The Congo Basin is the world's second largest area of contiguous tropical rainforest and second largest river basin in the world (Fig. 1), covering an area of 3.7 $x10^6$ km^2, with a mean discharge of around 42,000 m^{-3} s^{-1} (O'Loughlin et al., 2013) and a variation between 24,700–75,500 m^{-3} s^{-1} across months (Coynel et al., 2005).

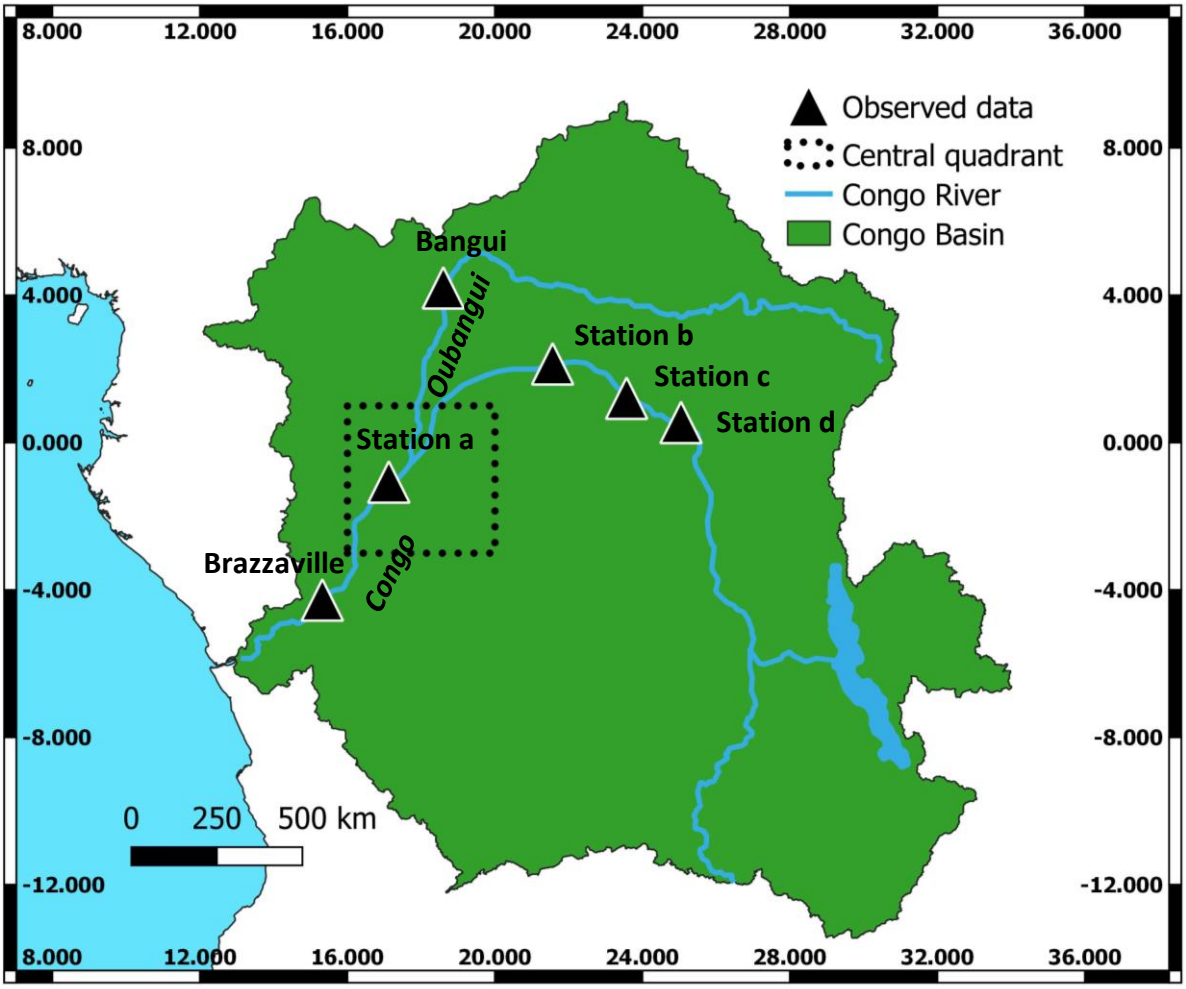

Figure 1:Extent of the Congo Basin, central quadrant of the "Cuvette Centrale" and sampling stations (for DOC and discharge) along the Congo and Oubangui Rivers (in italic).

The major climate (ISMSIP2b, Frieler et al., 2017; Lang et al., 2017) and land-cover (LUH-CMIP5) characteristics of the Congo Basin for the present day (1981-2010) are shown in Figure 2. The mean annual temperature is 25.2 °C but with considerable spatial variation from a low of 18.4°C to a high of 27.2°C (Fig. 2 a), while mean annual rainfall is 1520mm, varying from 733 mm to 4087 mm (Fig. 2 b). ORCHILEAK prescribes 13 different plant functional types (PFTs). Land-use is mixed with tropical broad-leaved evergreen (PFT2, Fig. 1 c), tropical broad-leaved rain green (PFT3, Fig. 1 d), C_3 grass (PFT10, Fig. 2 e) and C_4 grass (PFT11, Fig. 2 f) covering a maximum of 26%, 35%, 8% and 25% of the basin area respectively (Table A3). Most published estimates for land-cover follow national boundaries and so we can make broad

178 comparisons with published estimates for the Democratic Republic of Congo (DRC). For
179 example, our value for total forest cover for the DRC (65%), is close to the 67% and 68%
180 values estimated by the Congo Basin Forest Partnership (CBFP, 2009), and Potapov et al.
181 (2012), respectively. Agriculture covers only a small proportion of the basin according to the
182 LUH dataset that is based on FAO cropland area statistics, with C3 (PFT12, Fig. 2 g) and C_4
183 (PFT13, Fig. 2 h) agriculture making up a maximum basin area of 0.5 and 2% respectively. In
184 reality, a larger fraction of the basin is composed of small scale and rotational agriculture
185 (Tyukavina et al., 2018). The ORCHILEAK model also has a "poor soils" forcing file (Fig. 2
186 j) which prescribes reduced decomposition rates in soils with low nutrient and pH soils such as
187 Podzols and Arenosols (Lauerwald et al., 2017). This file is developed from the Harmonized
188 World Soil Database (FAO/IIASA/ISRIC/ISS-CAS/JRC, 2009).

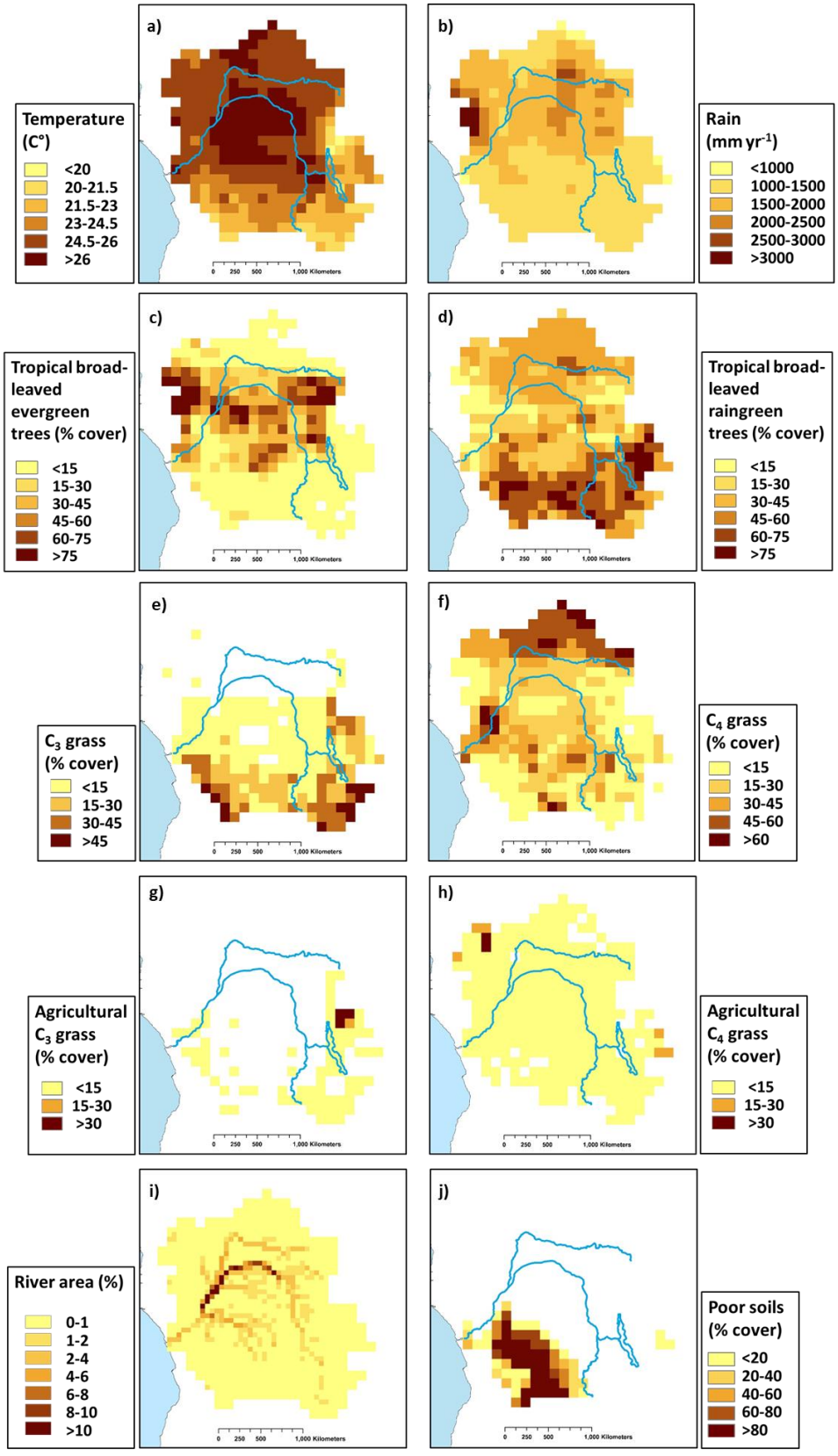

Figure 2: Present day (1981-2010) spatial distribution of the principal climate and land-use drivers used in ORCHILEAK, across the Congo Basin; a) mean annual temperature in °C, b) mean annual rainfall in mm yr^{-1}, c)-h) mean annual maximum vegetated fraction for PFTs 2,3,

10,11,12 and 13, i) river area, and j) Poor soils. All at a resolution of 1° except for river area (0.5°).

2.2 Development of floodplains and swamps forcing files

In ORCHILEAK, water in the river network can be diverted to two types of wetlands, floodplains and swamps. In each grid where a floodplain exists, a temporary waterbody can be formed adjacent to the river and is fed by the river once bank-full discharge (see section 2.3) is exceeded. In grids where swamps exist, a constant proportion of river discharge is fed into the base of the soil column; ORCHILEAK does not explicitly represent a groundwater reservoir and so this imitates the hydrological coupling of swamps and rivers through the groundwater table. The maximal proportions of each grid which can be covered by floodplains and swamps are prescribed by the maximal fraction of floodplains (MFF) and the maximal fraction of swamps (MFS) forcing files respectively (Guimberteau et al., 2012). See also Lauerwald et al. (2017) and Hastie et al. (2019) for further details. We created an MFF forcing file for the Congo basin, derived from the Global Wetlands^{v3} database; the 232 m resolution tropical wetland map of Gumbricht et al. (2017) (Fig. 3 a and b). We firstly amalgamated all the categories of wetland (which include floodplains and swamps) before aggregating them to a resolution of 0.5° (the resolution at which the floodplain/swamp forcing files are read by ORCHILEAK), assuming that this represents the maximum extent of inundation in the basin. This results in a mean MFF of 10%, i.e. a maximum of 10% of the surface area of the Congo basin can be inundated with water. This is identical to the mean MFF value of 10% produced with the Global Lakes and Wetlands Database, GLWD (Lehner, & Döll, P.,2004; Borges et al., 2015^{b}). We also created an MFS forcing file from the same dataset (Fig. 3 c and d), merging the ‘swamps’ and ‘fens’ wetland categories (although note that there are virtually no fens in the Congo basin) from Global Wetlands^{v3} database (Gumbricht et al., 2017) and again aggregating them to a 0.5° resolution. Please see Table 1 of Gumbricht et al. (2017) for further details.

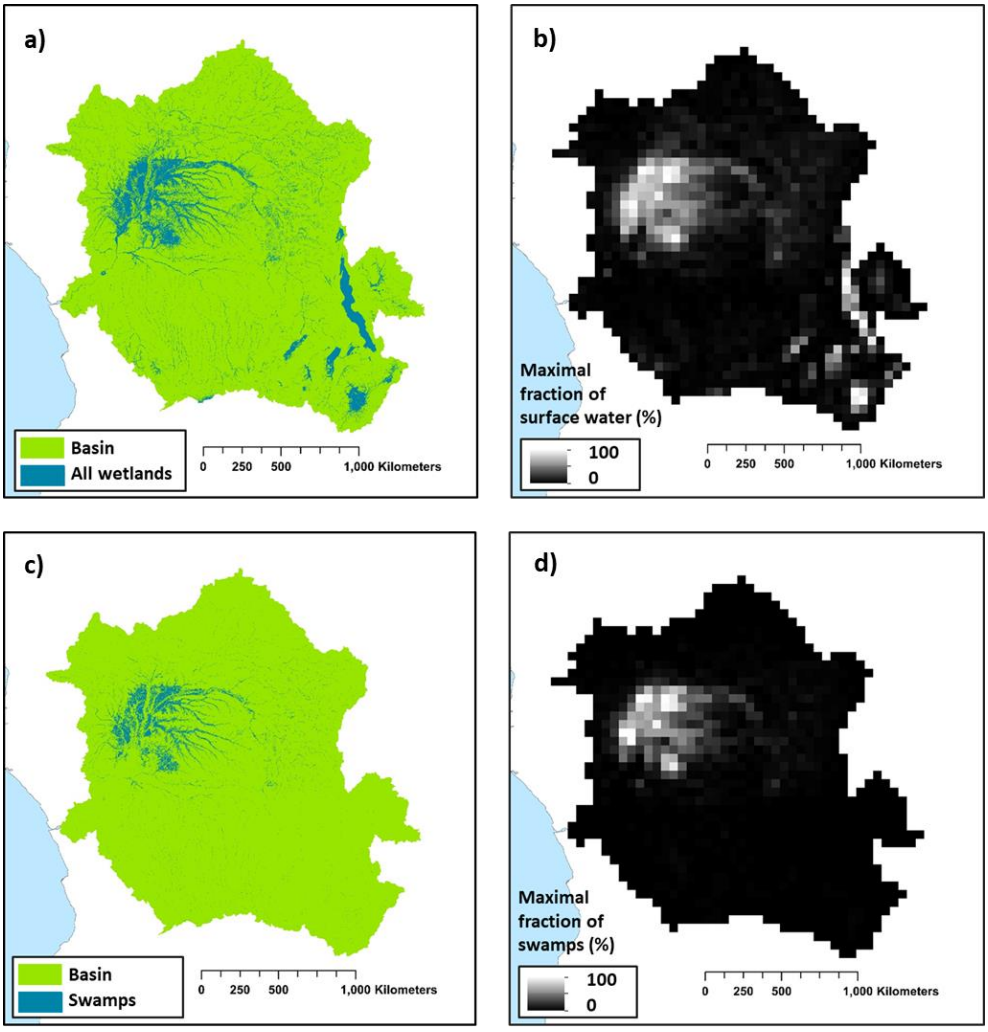

Figure 3: a) Wetland extent (from Gumbricht et al., 2017). b) The new maximal fraction of floodplain (MFF) forcing file developed from a). c) Swamps (including fens) category within Congo basin from Gumbricht et al (2017). d) the new maximal fraction of swamps (MFS) forcing file developed from c). Panels a) and b) are at the same resolution as the Gumbricht dataset (232m) while b) and d) are at a resolution of 0.5°. Note that 0.5° is the resolution of the sub unit basins in ORCHILEAK (Lauerwald et al., 2015), with each 1° grid containing four sub basins.

218

219 2.3 Calibration of hydrology

220 As the main driver of the export of C from the terrestrial to aquatic system, it is crucial that the
221 model can represent present-day hydrological dynamics, at the very least on the main stem of
222 the Congo. As this study is primarily concerned with decadal- centennial timescales our priority
223 was to ensure that the model can accurately recreate observed mean annual discharge at the
224 most downstream gauging station Brazzaville. We also tested the model's ability to simulate

observed discharge seasonality, as well as flood dynamics. Moreover, no data is available with which to directly evaluate the simulation of DOC and CO_2 leaching from the soil to the river network, and thus we tested the model's ability to recreate the spatial variation of observed riverine DOC concentrations and pCO_2 at specific stations where measurements are available (Borges at al., 2015[b]; Bouillon et al., 2012 & 2014, locations shown in Fig. 1), river DOC and CO_2 concentration being regarded as an integrator of the C transport at the terrestrial-aquatic interface.

We first ran the model for the present-day period, defined as from 1990 to 2005/2010 depending on which climate forcing data was applied, using four climate forcing datasets; namely ISIMIP2b (Frieler et al., 2017), Princeton GPCC (Sheffield et al., 2006), GSWP3 (Kim, 2017) and CRUNCEP (Viovy, 2018). We used ISIMIP2b for the historical and future simulations as it is the only climate forcing dataset to cover the full period (1861-2099). However, we compared it to other climate forcing datasets for the present day in order to gauge its ability to simulate observed discharge on the Congo River at Brazzaville (Table A1). Without calibration, the majority of the different climate forcing model runs performed poorly, unable to accurately represent the seasonality and mean monthly discharge at Brazzaville (Table A1). The best performing climate forcing dataset was ISIMIP2b followed by Princeton GPCC with root mean square errors (RMSE) of 29% and 40% and Nash Sutcliffe efficiencies (NSE) of 0.20 and -0.25, respectively. NSE is a statistical coefficient specifically used to test the predictive skill of hydrological models (Nash & Sutcliffe, 1970).

For ISIMIP2b we further calibrated key hydrological model parameters, namely the constants which dictate the water residence time of the groundwater (=slow reservoir), headwaters (= fast reservoir) and floodplain reservoirs in order to improve the simulation of observed discharge at Brazzaville (Table 2). To do so, we tested different combinations of water residence times for the three reservoirs, eventually settling on 1, 0.5 and 0.5 (days) for the slow,

fast and floodplain reservoirs respectively, all three being reduced compared to those values used in the original ORCHILEAK calibration for the Amazon (Lauerwald at al., 2017).

In order to calibrate the simulated discharge against observations, we first modified the flood dynamics of ORCHILEAK in the Congo Basin for the present day by adjusting bank-full discharge ($streamr_{50th}$, Lauerwald et al., 2017) and 95th percentile of water level heights ($floodh_{95th}$). As in previous studies on the Amazon basin (Lauerwald et al. 2017, Hastie et al., 2019) we defined bank-full discharge, i.e. the threshold discharge at which floodplain inundation starts (i.e. overtopping of banks), as the median discharge (50th percentile i.e. $streamr_{50th}$) of the present-day climate forcing period (1990 to 2005). After re-running each model parametrization (different water residence times) to obtain those bank-full discharge values, we calculated $floodh_{95th}$ over the simulation period for each grid cell (Table 1). This value is assumed to represent the water level over the river banks at which the maximum horizontal extent of floodplain inundation is reached. We then ran the model for a final time and validated the outputs against discharge data at Brazzaville (Cochonneau et al., 2006, Fig. 1). This procedure was repeated iteratively with the ISIMIP2b climate forcing, modifying the water residence times of each reservoir in order to find the best performing parametrization.

We firstly compared simulated versus observed discharge at Brazzaville (NSE, RMSE, Table 2), before using the data of Bouillon et al. (2014) to further validate discharge at Bangui (Fig. 1) on the main tributary Oubangui. In addition, we compared the simulated seasonality of flooded area against the satellite derived dataset GIEMS (Prigent et al., 2007; Becker et al., 2018), within the Cuvette Centrale wetlands (Fig. 1).

2.4 Simulation set-up

A list of the main forcing files used, along with data sources, is presented in Table 1. The derivation of the floodplains and swamp (MFF & MFS) is described in section 2.2 while the

calculation of "bankfull discharge" ($streamr_{50th}$) and "95th percentile of water table height over flood plain" ($floodh_{95th}$) (Table 1) is described in section 2.3.

2.4.1 Soil carbon spin up

ORCHILEAK includes a soil module, primarily derived from ORCHIDEE-SOM (Camino Serrano, 2018). The soil module has 3 different pools of soil DOC; the passive, slow and active pool and these are defined by their source material and residence times (τ_{carbon}). ORCHILEAK also differentiates between flooded and non-flooded soils; decomposition rates of DOC, SOC and litter being reduced (3 times lower) in flooded soils. In order for the soil C pools to reach steady state, we spun-up the model for around 9,000 years, with fixed land-use representative of 1861, and looping over the first 30 years of the ISMSIP2b climate forcing data (1861-1890). During the first 2,000 years of spin-up, we ran the model with an atmospheric CO_2 concentration of 350 µatm and default soil C residence times (τ_{carbon}) halved, which allowed it to approach steady-state more rapidly. Following this, we ran the model for a further 7,000 years reverting to the default τ_{carbon} values. At the end of this process, the soil C pools had reached approximately steady state; <0.02% change in each pool over the final century of the spin-up.

2.4.2 Transient simulations

After the spin-up, we ran a historical simulation from 1861 until the present day, 2005 in the case of the ISIMIP2b climate forcing data. We then ran a future simulation until 2099, using the final year of the historical simulation as a restart file. In both of these simulations, climate, atmospheric CO_2 and land-cover change were prescribed as fully transient forcings according to the RCP6.0 scenario. For climate variables, we used the IPSL-CM5A-LR model outputs for RCP 6.0, bias corrected by the ISIMIP2b procedure (Frieler et al., 2017; Lange et al., 2017), while land-use change was taken from the 5th Coupled Model Intercomparison Project (CMIP5). As our aim is to investigate long-term trends, we calculated 30-years running means

of simulated C flux outputs in order to smooth interannual variations. RCP 6.0 is an emissions pathway that leads to a "stabilization of radiative forcing at 6.0 Watts per square meter (Wm^{-2}) in the year 2100 without exceeding that value in prior years" (Masui et al., 2011). It is characterised by intermediate energy intensity, substantial population growth, mid-high C emissions, increasing cropland area to 2100 and decreasing natural grassland area (van Vuuren et al., 2011). In the paper which describes the development of the future land use change scenarios under RCP 6.0 (Hurtt et al., 2011), it is shown that land use change is highly sensitive to land use model assumptions, such as whether or not shifting cultivation is included. The LUH1 reconstruction for instance indicates shifting cultivation affecting all of the tropics with a residence time of agriculture of 15 years, whereas the review from Heinimann et al. (2017) revised downwards the area of this type of agriculture, with generally low values in Congo, except in the North East and South East, but suggested a shorter turnover of agriculture of two years only. In view of such uncertainties, we did not include shifting agriculture in the model. Moreover, there is considerable uncertainty associated with the effect of future land-use change in Africa (Hurtt et al., 2011). We chose RCP 6.0 as it represents a no mitigation (mid-high emissions) scenario. Moreover, the ISIMIP2b data only provided two RCPs at the time we performed the simulations; RCP 2.6 (low emission) and RCP 6.0.

With the purpose of evaluating separately the effects of land-use change, climate change, and rising atmospheric CO_2, we ran a series of factorial simulations. In each simulation, one of these factors was fixed at its 1861 level (the first year of the simulation), or in the case of fixed climate change, we looped over the years 1861-1890. The outputs of these simulations (also 30-year running means) were then subtracted from the outputs of the main simulation (original run with all factors varied) so that we could determine the contribution of each driver (Fig. 10, Table 1).

Table 1:Main forcing files used for simulations

Variable	Spatial resolution	Temporal resolution	Data source
Rainfall, snowfall, incoming shortwave and longwave radiation, air temperature, relative humidity and air pressure (close to surface), wind speed (10 m above surface)	1°	1 day	ISIMIP2b, IPSL-CM5A-LR model outputs for RCP6.0 (Frieler et al., 2017)
Land cover (and change)	0.5°	annual	LUH-CMIP5
Poor soils	0.5°	annual	Derived from HWSD v 1.1 (FAO/IIASA/ISRIC/ISS-CAS/JRC, 2009)
Stream flow directions	0.5°	annual	STN-30p (Vörösmarty et al., 2000)
Floodplains and swamps fraction in each grid (MFF & MFS)	0.5°	annual	derived from the wetland high resolution data of Gumbricht et al. (2017)
River surface areas	0.5°	annual	Lauerwald et al. (2015)
Bankfull discharge ($streamr_{50th}$)	1°	annual	derived from calibration with ORCHILEAK (see section 2,3)
95th percentile of water table height over flood plain ($floodh_{95th}$)	1°	annual	derived from calibration with ORCHILEAK (see section 2.3)

2.5 Evaluation and analysis of simulated fluvial C fluxes

We first evaluated DOC concentrations and pCO_2 at several locations along the Congo mainstem (Fig. 1), and on the Oubangui river against the data of Borges at al. (2015[b]) and Bouillon et al. (2012, 2014) We also compared the various simulated components of the net C balance (e.g. NPP) of the Congo against values described in the literature (Williams et al., 2007; Lewis et al., 2009; Verhegghen et al., 2012; Valentini et al., 2014; Yin et al., 2017). In addition, we assessed the relationship between the interannual variation in present day (1981-2010) C fluxes of the Congo basin and variation in temperature and rainfall. This was done through linear regression using STATISTICA™. We found trends in several of the fluxes over the 30-year period (1981-2010) and thus detrended the time series with the "Detrend" function, part of the "SpecsVerification" package in R (R Core Team 2013), before undertaking the statistical analysis focused on the climate drivers of inter-annual variability.

2.6 Calculating the net carbon balance of the Congo basin

We calculated Net Ecosystem Production (NEP) by summing the terrestrial and aquatic C fluxes of the Congo basin (Eq. 1), while we incorporated disturbance fluxes (Land-use change flux and harvest flux) to calculate Net Biome Production (NBP) (Eq. 2). Positive values of NBP and NEP equate to a net terrestrial C sink.

NEP is defined as follows:

$$NEP = NPP + TF - SHR - FCO_2 - LE_{\text{Aquatic}} \quad (1)$$

Where *NPP* is terrestrial net primary production, *TF* is the throughfall flux of DOC from the canopy to the ground, *SHR* is soil heterotrophic respiration (only that evading from the *terra-firme* soil surface); FCO_2 is CO_2 evasion from the water surface and $LE_{Aquatic}$ is the lateral export flux of C (DOC + dissolved CO_2) to the coast. NBP is equal to NEP except with the inclusion of the C lost (or possibly gained) via land use change (*LUC*) and crop harvest (*HAR*). Wood harvest is not included for logging and forestry practices, but during deforestation LUC, a fraction of the forest biomass is harvested and channelled to wood product pools with different decay constants. *LUC* includes land conversion fluxes and the lateral export of wood products biomass, that is, assuming that wood products from deforestation are not consumed and released as CO_2 over the Congo, but in other regions:

$$NBP = NEP - (LUC + HAR) \quad (2)$$

3. Results

3.1 Simulation of hydrology and aquatic carbon fluxes

The final model configuration is able to closely reproduce the mean monthly discharge at Brazzaville (Fig. 4 a), Table 2) and captures the seasonality moderately well (Fig. 4 a, Table 2,

RMSE =23%, R^2 =0.84 versus RMSE= 29% and R^2 =0.23 without calibration, Table A1). At Bangui on the Oubangui River (Fig. 1), the model is able to closely recreate observed seasonality (Fig. 4 b), RMSE =59%, R^2 =0.88) but substantially underestimates the mean monthly discharge, our value being only 50% of the observed. We produce reasonable NSE values of 0.66 and 0.31 for Brazzaville and Bangui respectively, indicating that the model is moderately accurate in its simulation of seasonality.

We also evaluated the simulated seasonal change in flooded area in the central (approx. 200,000 km^2, Fig. 1) part of the Cuvette Centrale wetlands against the GIEMS inundation dataset (1993-2007, maximum inundation minus minimum or permanent water bodies, Prigent et al., 2007; Becker et al., 2018). While our model is able to represent the seasonality in flooded area relatively well (R^2 =0.75 Fig. 4 c), it considerably overestimates the magnitude of flooded area relative to GIEMS (Fig. 4 c, Table 2). However, the dataset that we used to define the MFF and MFS forcing files (Gumbricht et al., 2017) is produced at a higher resolution than GIEMS and will capture smaller wetlands than the GIEMS dataset, and thus the greater flooded area is to be expected. GIEMS is also known to underestimate inundation under vegetated areas (Prigent et al., 2007; Papa et al., 2010) and has difficulties to capture small inundated areas (Prigent et al., 2007; Lauerwald et al., 2017). Indeed, with the GIEMS data we produce an overall flooded area for the Congo Basin of just 3%, less than one-third of that produced with the Gumbricht dataset (Gumbricht et al., 2017) or the GLWD (Lehner, & Döll, P.,2004). As such, it is to be expected that there is a large RMSE (272%, Table 2) between simulated flooded area and GIEMS; more importantly, the seasonality of the two is highly correlated (R^2 = 0.67, Table 2).

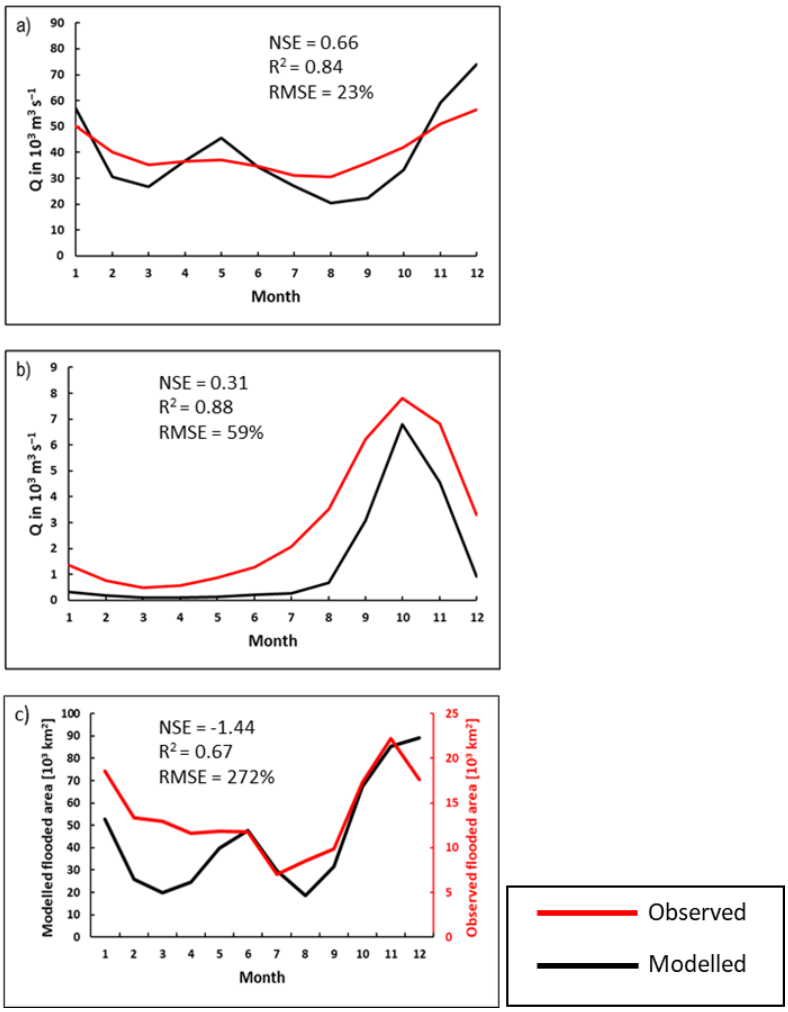

Figure 4: Seasonality of simulated versus observed discharge at a) Brazzaville on the Congo (Cochonneau et al., 2006), b) Bangui on the Oubangui (Bouillon et al., 2014) 1990-2005 monthly mean and c) flooded area in the central (approx. 200,000 km^2) area of the Cuvette Centrale wetlands versus GIEMS (1993-2007, Becker et al., 2018). The observed flooded area data represents the maximum minus minimum (permanent water bodies such as rivers) GIEMS inundation. See Figure 1 for locations.

Table 2: Performance statistics for modelled versus observed seasonality of discharge and flooded area in Cuvette Centrale

Station	RSME	NSE	R^2	Simulated mean monthly discharge ($m^3\ s^{-1}$)	Observed mean monthly discharge ($m^3\ s^{-1}$)
Brazzaville	23%	0.66	0.84	38,944	40,080
Bangui	59%	0.31	0.88	1,448	2,923
				Simulated mean monthly flooded area ($10^3\ km^2$)	Observed mean monthly flooded area ($10^3\ km^2$)
Flooded area (Cuvette Centrale)	272%	-1.44	0.67	44	14

In Figure 5, we compare simulated DOC concentrations at six locations (Fig. 1) along the Congo River and Oubangui tributary, against the observations of Borges at al. (2015[b]). We show that we can recreate the spatial variation in DOC concentration within the Congo basin relatively closely with an R^2 of 0.74 and an RMSE of 24% (Fig. 5). We are also able to simulate the broad spatial pattern of pCO_2 measured in Borges et al. (2019). During high flow season (mean of 6 consecutive months of highest flow, 2009-2019) we simulate a mean pCO_2 of 3,373 ppm and 5,095 ppm at Kisangani and Kinshasa (Brazzaville) respectively, compared to the observed values of 2,424 ppm and 5,343 ppm during high water (measured in December 2013, Borges et al., 2019) (Table 3). Similarly, during low flow season (mean of 6 consecutive months of lowest flow, 2009-2019) we simulate a mean pCO_2 of 1,563 ppm and 2,782 ppm at Kisangani and Kinshasa respectively, compared to the observed values of 1,670 ppm and 2,896 ppm during falling water (June 2014, Borges et al., 2019) (Table 3).

While we are able to recreate observed spatial differences in DOC and pCO_2, as well as broad seasonal variations, we are not able to correctly predict the exact timing of the simulated highs and lows, a reflection of not fully capturing the hydrological seasonality. For example, our mean June pCO_2 at Kinshasa (Brazzaville) is 4,470 ppm, while Borges et al measured a mean of 2,896 ppm (Table 3). However, our value for July of 2,621 ppm is much closer, and moreover our mean value for December of 5,154 ppm is relatively close to the observed value of 5,343 ppm. Similarly, we fail to predict the timing of the June falling water at Kisangani (Table 3).

In Figure 6, we compare simulated pCO_2 against the observed monthly time series at Bangui on the Oubangui River (Bouillon et al., 2012 & 2014), as far as we are aware the most complete time series of pCO_2 published from the Congo basin, spanning March 2010 to March 2012 (with only the single month of June 2010 missing). Again, while the model fails to correctly predict the precise timing of the peak as with the Kinshasa and Kisangani datasets the broad seasonal variation in pCO_2 is captured, with the observed and modelled times series ranging from 227- 4040 ppm and 415- 2928 ppm, respectively (Fig. 6).

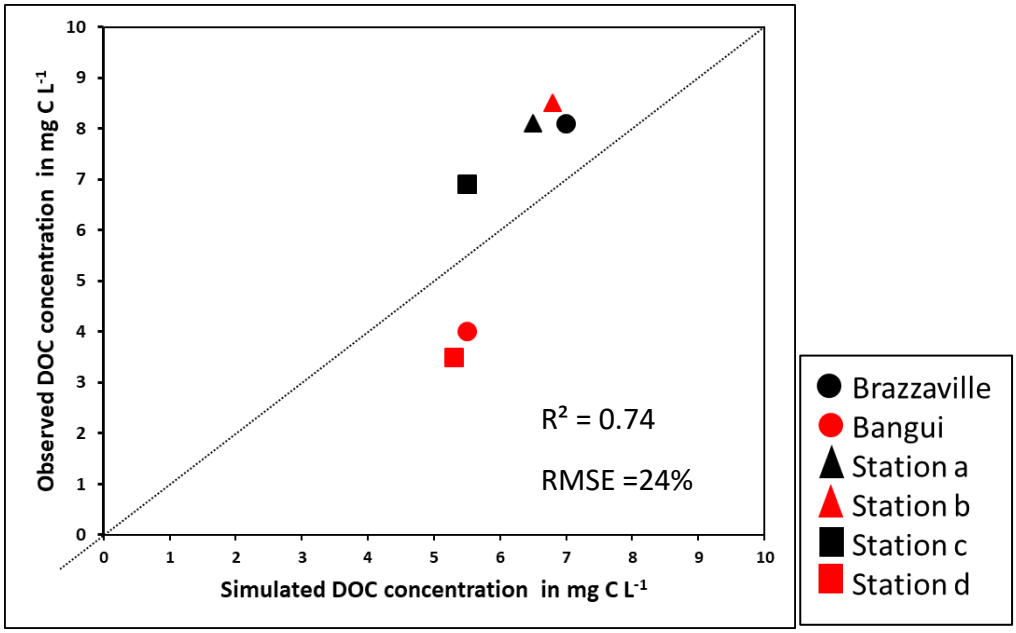

420

Figure 5: Observed (Borges et al., 2015[a]) versus simulated DOC concentrations at several sites along the Congo and Oubangui rivers. See Fig. 1 for locations. The simulated and observed DOC concentrations represent the median values across the particular sampling period at each location detailed in Borges et al. (2015[a]).

421

Table 3: Observed (Borges et al., 2019) and modelled pCO_2 (in ppm) at Kinshasa (Brazzaville) and Kisangani on the Congo river at various water levels.

Location	Observed pCO_2 highwater (December 2013)	Modelled pCO_2 highwater (December Mean 2009-2019)	Modelled pCO_2 high flow season (mean of 6 consecutive months of highest flow 2009-2019)	Observed pCO_2 falling water (June 2014)	Modelled pCO_2 falling water (June mean 2009-2019)	Modelled pCO_2 low flow season (mean of 6 consecutive months of lowest flow 2009-2019)
Kinshasa (Brazzaville)	5,343	5,154	5,095	2,896	4,470	2,782
Kisangani	2,424	2,166	3,373	1,670	3,126	1,563

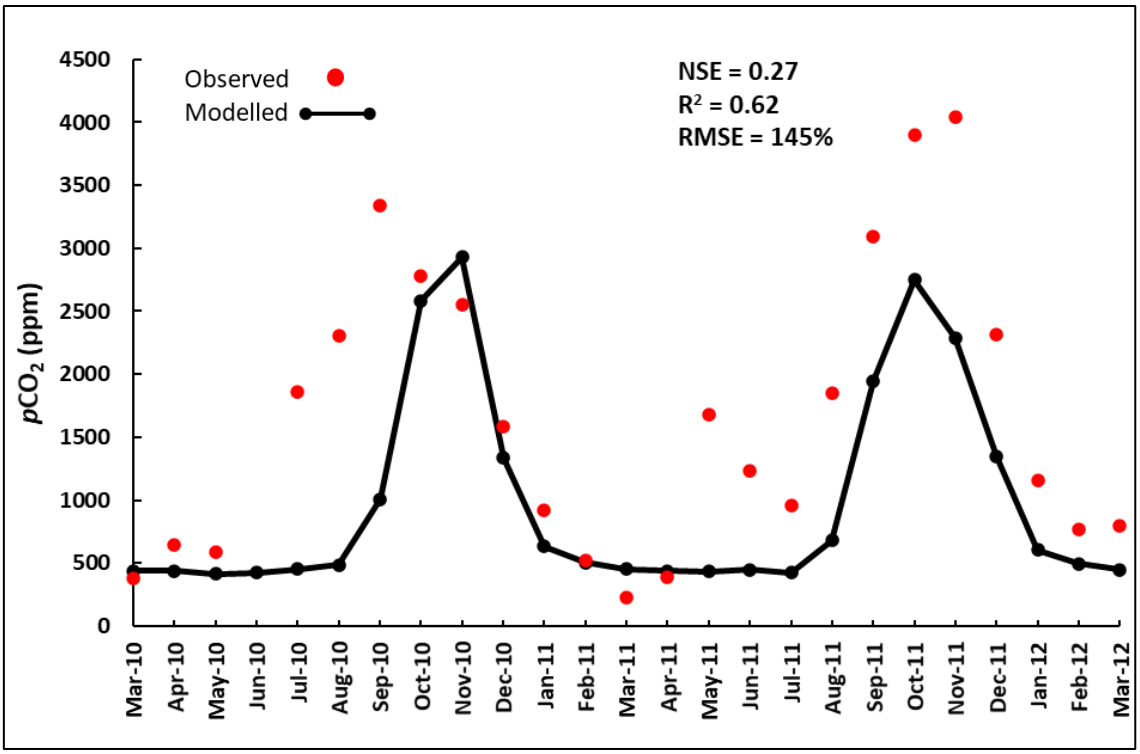

Figure 6: Time series of observed *versus* simulated pCO_2 at Bangui on the River Oubangui. Observed data is from Bouillon et al., 2012 and Bouillon et al., 2014.

3.2 Carbon fluxes along the Congo basin for the present day

For the present day (1981-2010) we estimate a mean annual terrestrial net primary production (NPP) of 5,800 ±166 (standard deviation, SD) Tg C yr^{-1} (Fig. 7), corresponding to a mean areal C fixation rate of approximately 1,500 g C m^{-2} yr^{-1} (Fig. 8 a). We find a significant positive correlation between the interannual variation of NPP and rainfall (detrended R^2= 0.41, $p<0.001$, Table A2) and a negative correlation between annual NPP and temperature (detrended R^2= 0.32, $p<0.01$, Table A2). We also see considerable spatial variation in NPP across the Congo Basin (Fig.8 a).

We simulate a mean soil heterotrophic respiration (SHR) of 5,300 ±99 Tg C yr^{-1} across the Congo basin (Fig. 7). Contrary to NPP, interannual variation in annual SHR is positively correlated with temperature (detrended R^2= 0.57, p<0.0001, Table A2) and inversely correlated with rainfall (detrended R^2= 0.10), though the latter relationship is not significant (p>0.05). We estimate a mean annual aquatic CO_2 evasion rate of 1,363 ±83 g C m^{-2} yr^{-1}, amounting to a total of 235±54 Tg C yr^{-1} across the total water surfaces of the Congo basin (Fig. 7) and attribute 85% of this flux to flooded areas, meaning that only 32 Tg C yr^{-1} is evaded directly from the river surface. Interannual variation in aquatic CO_2 evasion (1981-2010) shows a strong positive correlation with rainfall (detrended R^2= 0.75, p<0.0001, Table A2) and a weak negative correlation with temperature (detrended R^2=0.09, not significant, p>0.05). Aquatic CO_2 evasion also exhibits substantial spatial variation (Fig.8, d), displaying a similar pattern to both terrestrial DOC leaching (DOC_{inp}) (R^2= 0.81, p<0.0001, Fig.8, b) as well as terrestrial CO_2 leaching (CO_{2inp}) (R^2= 0.96, p<0.0001, Fig.8, c) into the aquatic system, but not terrestrial NPP (R^2= 0.01, p<0.05, Fig.8, a). We simulate a mean annual flux of DOC throughfall from the canopy of 27 ±1 Tg C yr^{-1} and C (DOC + dissolved CO_2) export flux to the coast of 15 ±4 Tg C yr^{-1} (Fig. 7).

For the present day (1981-2010) we estimate a mean annual net ecosystem production (NEP) of 277 ±137 Tg C yr^{-1} and a net biome production (NBP) of 107 ±133 Tg C yr^{-1} (Fig. 7). Interannually, both NEP and NBP exhibit a strong inverse correlation with temperature (detrended NEP R^2=0.55, p<0.0001, detrended NBP R^2=0.54, p<0.0001) and weak positive relationship with rainfall (detrended NEP R^2=0.16, p<0.05, detrended NBP R^2=0.14, p<0.05). Furthermore, we simulate a present day (1981-2010) living biomass of 41 ±1 Pg C and a total soil C stock of 109 ±1 Pg C.

458

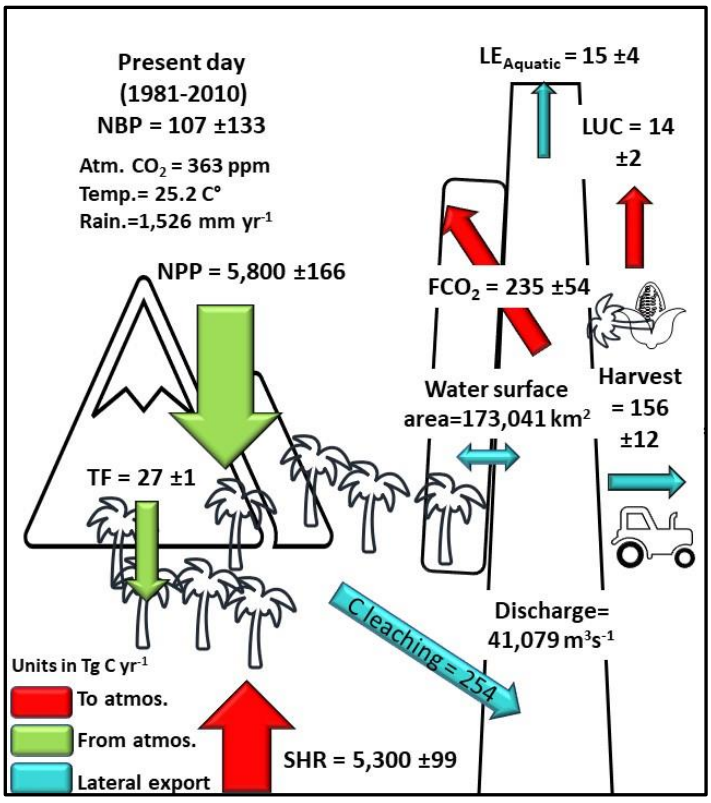

459

Figure 7: Annual C budget (NBP) for the Congo basin for the present day (1981-2010) simulated with ORCHILEAK, where NPP is terrestrial net primary productivity, TF is throughfall, SHR is soil heterotrophic respiration, FCO_2 is aquatic CO_2 evasion, LOAC is C leakage to the land-ocean aquatic continuum (FCO_2 + $LE_{Aquatic}$), LUC is flux from Land-use change, and $LE_{Aquatic}$ is the export C flux to the coast. Range represents the standard deviation (SD) from 1981-2010.

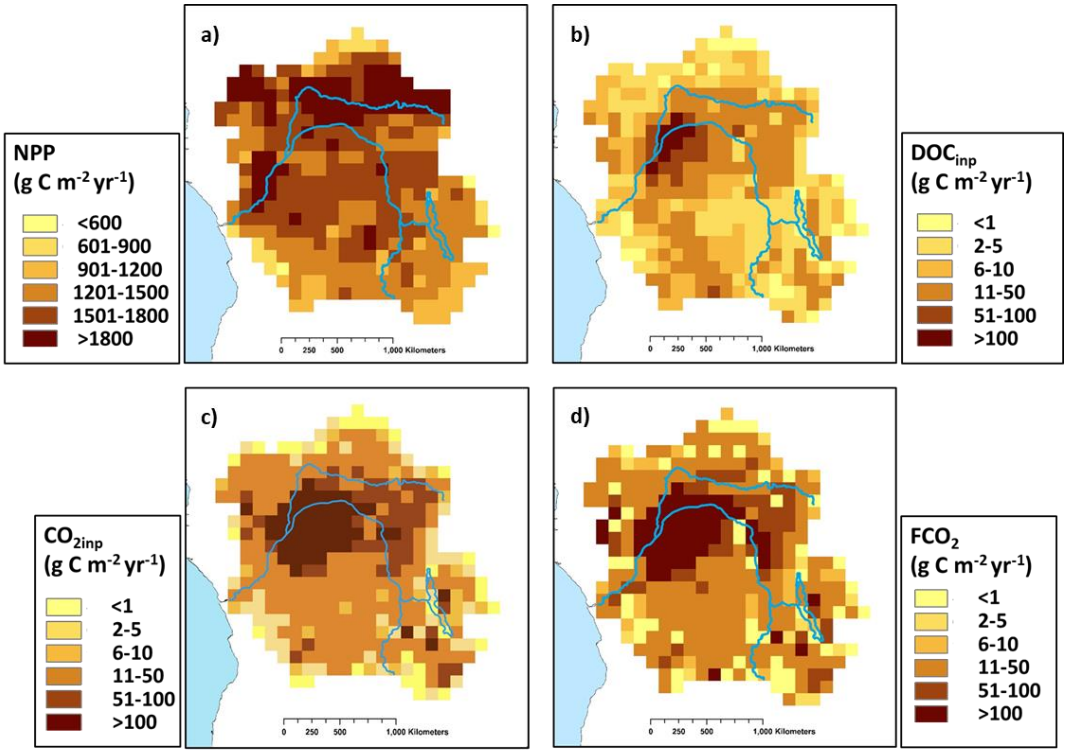

460

Figure 8:Present day (1981-2010) spatial distribution of a) terrestrial net primary productivity (NPP), b) dissolved organic carbon export from soils and floodplain vegetation into the aquatic system (DOC_{inp}), c) CO_2 leaching from soils and floodplain vegetation into the aquatic system (CO_{2inp}) and d) aquatic CO_2 evasion (FCO_2). Main rivers in blue. All at a resolution of 1°

461

462 3.3 Long-term temporal trends in carbon fluxes

463 We find an increasing trend in aquatic CO_2 evasion (Fig. 9 a) throughout the simulation period,
464 rising slowly at first until the 1960s when the rate of increase accelerates. In total CO_2 evasion
465 rose by 79% from 186 Tg C yr^{-1} at the start of the simulation (1861-1890 mean) (Fig. 10) to
466 333 Tg C yr^{-1} at the end of this century (2070-2099 mean, Fig. 10), while the increase until the
467 present day (1981-2010 mean) is of +26 % (to 235 Tg C yr^{-1}), though these trends are not
468 uniform across the basin (Fig A1). The lateral export flux of C to the coast ($LE_{Aquatic}$) follows
469 a similar relative change (Fig. 9b), rising by 67% in total, from 12 Tg C yr^{-1} (Fig. 10) to 15 Tg
470 C yr^{-1} for the present day, and finally to 20 Tg C yr^{-1} (2070-2099 mean, Fig. 10). This is greater
471 than the equivalent increase in DOC concentration (24%, Fig. 9b) due to the concurrent rise in
472 rainfall (by 14%, Fig 9h) and in turn discharge (by 29%, Fig. 9h).

Terrestrial NPP and SHR also exhibit substantial increases of 35% and 26% respectively across the simulation period and similarly rise rapidly after 1960 (Fig. 9c). NEP, NBP (Fig. 9d) and living biomass (Fig. 9 e) follow roughly the same trend as NPP, but NEP and NBP begin to slow down or even level-off around 2030 and in the case of NBP, we actually simulate a decreasing trend over approximately the final 50 years. Interestingly, the proportion of NPP lost to the LOAC also increases from approximately 3% to 5% (Fig. 9c). We also find that living biomass stock increases by a total of 53% from 1861 to 2099. Total soil C also increases over the simulation but only by 3% from 107 to 110 Pg C yr^{-1} (Fig. 9e). Emissions from land-use change (LUC) show considerable decadal fluctuation increasing rapidly in the second half of the 20^{th} century and decreasing in the mid-21^{st} century before rising again towards the end of the simulation (Fig. 9f). The harvest flux (Fig. 9f) rises throughout the simulation with the exception of a period in the mid-21^{st} century during which it stalls for several decades. This is reflected in the change in land-use areas from 1861- 2099 (Fig. A2, Table A3) during which the natural forest and grassland PFTs marginally decrease while both C_3 and C_4 agricultural grassland PFTs increase.

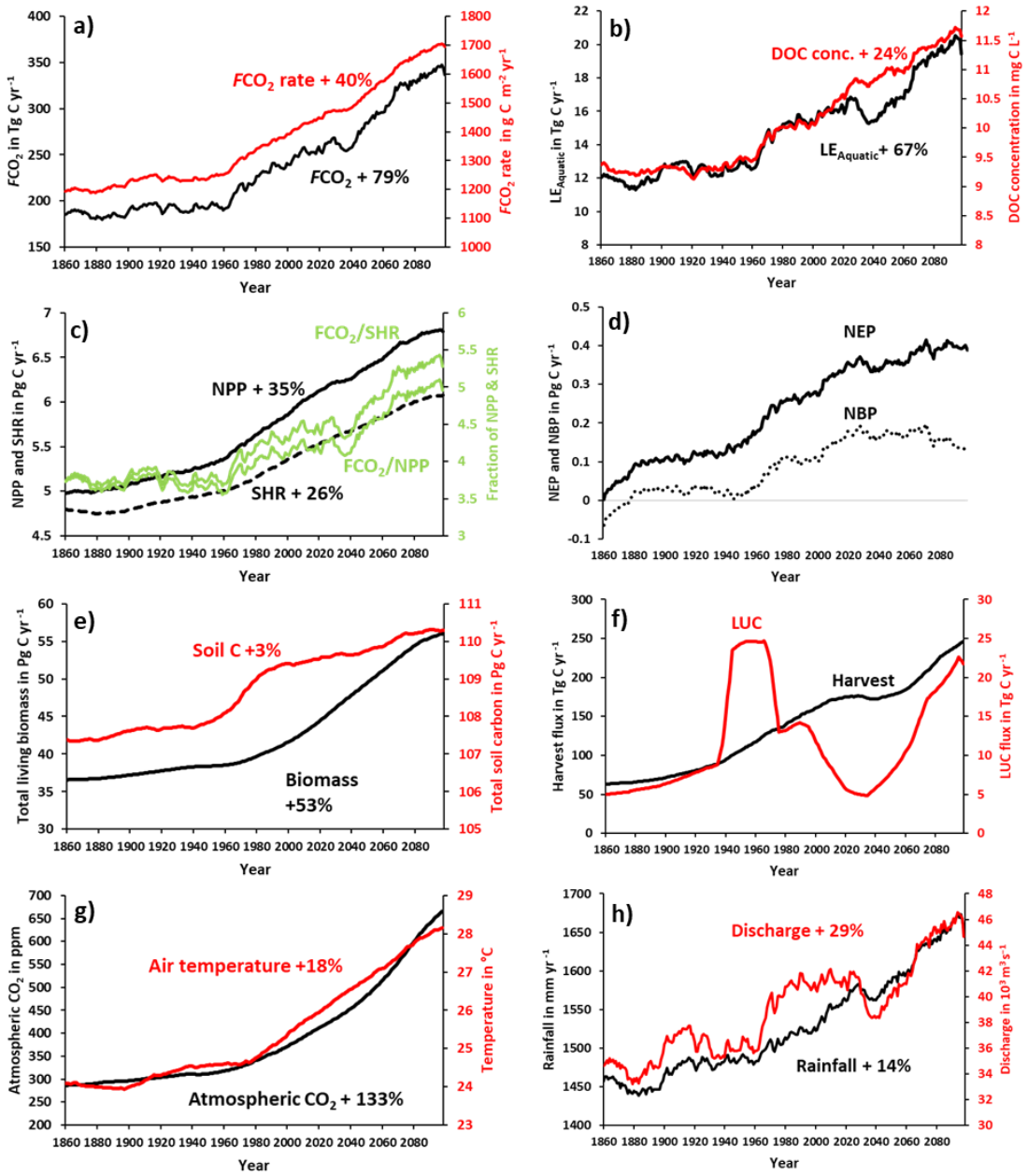

Figure 9: Simulation results for various C fluxes and stocks from 1861-2099, using IPSL-CM5A-LR model outputs for RCP 6.0 (Frieler et al., 2017). All panels except for atmospheric CO_2, biomass and soil C correspond to 30-year running means of simulation outputs. This was done in order to suppress interannual variation, as we are interested in longer-term trends.

3.4 Drivers of simulated trends in carbon fluxes

The dramatic increase in the concentration of atmospheric CO_2 (Fig. 9 g) and subsequent fertilization effect on terrestrial NPP has the greatest overall impact on all of the fluxes across

499 the simulation period (Fig. 11). It is responsible for the vast majority of the growth in NPP,
500 SHR, aquatic CO_2 evasion and flux of C to the coast (Fig. 11 a, b, c & d). The effect of LUC
501 on these four fluxes is more or less neutral, while the impact of climate change is more varied.
502 The aquatic fluxes (Fig. 11 c, d) respond positively to an acceleration in the increase of both
503 rainfall (and in turn discharge, Fig. 9 h) and temperature (Fig. 9 g) starting around 1970. From
504 around 2020, the impact of climate change on the lateral flux of C to the coast (Fig 11 d) reverts
505 to being effectively neutral, likely a response to a slowdown in the rise of rainfall and indeed a
506 decrease in discharge (Fig 9 h), as well as perhaps the effect of temperature crossing a
507 threshold. The response of the overall loss of terrestrial C to the LOAC (i.e. the ratio of
508 LOAC/NPP, Fig. 11 e) is relatively similar to the response of the individual aquatic fluxes but
509 crucially, climate change exerts a much greater impact, contributing substantially to an increase
510 in the loss of terrestrial NPP to the LOAC in the 1960s, and again in the second half of the 21st
511 century. These changes closely coincide with the pattern of rainfall and in particular with
512 changes in discharge (Fig. 9 h).

513 Overall temperature and rainfall increase by 18% and 14% from 24°C to 28°C and 1457mm to
514 1654mm respectively, but in Fig. A2 one can see that this increase is non-uniform across the
515 basin. Generally speaking, the greatest increase in temperature occurs in the south of the basin
516 while it is the east that sees the largest rise in rainfall (Fig. A2). Land-use changes are similarly
517 non-uniform (Fig. A2).

518 The response of NBP and in NEP (Fig.11 f, g) to anthropogenic drivers is more complex. The
519 simulated decrease in NBP towards the end of the run is influenced by a variety of factors;
520 LUC and climate begin to have a negative effect on NBP (contributing to a decrease in NBP)
521 at a similar time while the positive impact (contributing to an increase in NBP) of atmospheric
522 CO_2 begins to slow down and eventually level-off (Fig.11 g). LUC continues to have a positive
523 effect on NEP (Fig.11 f) due to the fact that the expanding C_4 crops have a higher NPP than

forests, while it has an overall negative effect on NBP at the end of the simulation due to the inclusion of emissions from crop harvest.

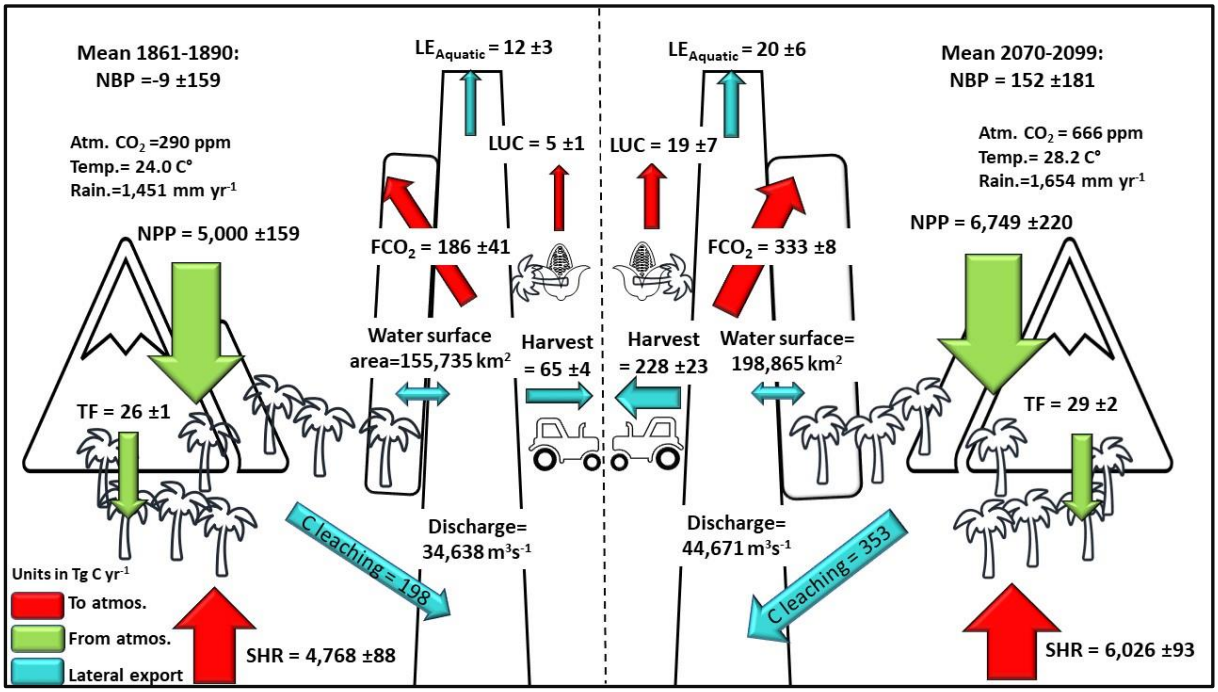

Figure 10: Annual C budget (NBP) for the Congo basin for; left, the Year 1861 and right, the Year 2099, simulated with ORCHILEAK. NPP is terrestrial net primary productivity, TF is throughfall, SHR is soil heterotrophic respiration, FCO_2 is aquatic CO2 evasion, LOAC is C leakage to the land-ocean aquatic continuum (FCO_2 + $LE_{Aquatic}$), LUC is flux from Land-use change, and $LE_{Aquatic}$ is the export C flux to the coast. Range represents the standard deviation (SD).

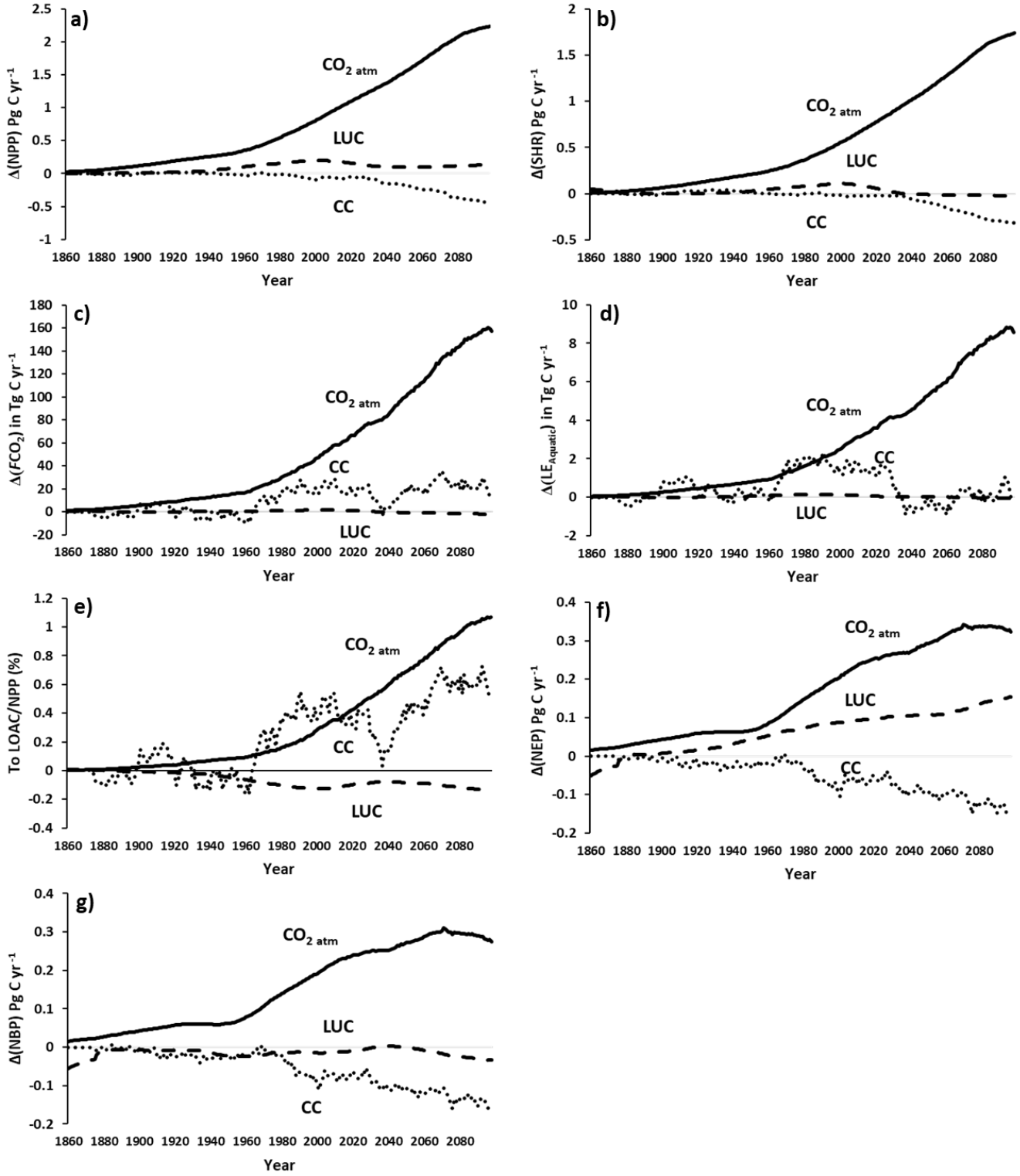

Figure 11: Contribution of anthropogenic drivers; atmospheric CO_2 concentration ($CO_{2\ atm}$), climate change (CC) and land use change (LUC) to changes in the various carbon fluxes along the Congo Basin, under IPSL-CM5A-LR model outputs for RCP 6.0 (Frieler et al., 2017).

4. Discussion

4.1 Congo basin carbon balance

We simulate a mean present-day terrestrial NPP of approximately 1,500 g C m^{-2} yr^{-1} (Fig. 6), substantially larger than the MODIS derived value of around 1,000 g C m^{-2} yr^{-1} from Yin et al. (2017) across central Africa, though it is important to note that satellite derived estimates of NPP can underestimate the impact of CO_2 fertilization, namely its positive effect on photosynthesis (De Kauwe et al., 2016; Smith et al., 2019). Our stock of the present-day living biomass of 41.1 Pg C is relatively close to the total Congo vegetation biomass of 49.3 Pg C estimated by Verhegghen et al. (2012) based on the analysis of MERIS satellite data. Moreover, our simulated Congo Basin soil C stock of 109 ±1.1 Pg C is consistent with the approximately 120-130 Pg C across Africa between the latitudes 10°S to 10°N in the review of Williams et al. (2007), between which the Congo represents roughly 70% of the land area. Therefore, their estimate of soil C stocks across the Congo only would likely be marginally smaller than ours. It is also important to note that neither estimate of soil C stocks explicitly take into account the newly discovered peat store of 30 Pg C (Dargie et al., 2017) and therefore both are likely to represent conservative values. In addition, Williams et al. (2007) estimate the combined fluxes from conversion to agriculture and cultivation to be around 100 Tg C yr^{-1} in tropical Africa (largely synonymous with the Congo Basin), which is relatively close to our present day estimate of harvesting + land-use change flux of 170 Tg C yr^{-1}.

Our results suggest that CO_2 evasion from the water surfaces of the Congo is sustained by the transfer of dissolved CO_2 and DOC with 226 Tg C and 73 Tg C, respectively, from wetland soils and vegetation to the aquatic system each year (1980-2010, Fig. 8). Moreover, we find that a disproportionate amount of this transfer occurs within the Cuvette Centrale wetland (Fig. 1, Fig. 8) in the centre of the basin, in agreement with a recent study by Borges et al. (2019). In our study, this is due to the large areal proportion of inundated land, facilitating the exchange

between soils and aquatic systems. Borges et al. (2019) conducted measurements of DOC and pCO_2, amongst other chemical variables, along the Congo mainstem and its tributaries from Kinshasa in the West of the basin (beside Brazzaville, Fig. 1) through the Cuvette Centrale to Kisangani in the East (close to station d in Fig. 1). They found that both DOC and pCO_2 approximately doubled from Kisangani downstream to Kinshasa (Table 3), and demonstrated that this variation is overwhelmingly driven by fluvial-wetland connectivity, highlighting the importance of the vast Cuvette Centrale wetland in the aquatic C budget of the Congo basin.

Our estimate of the integrated present-day aquatic CO_2 evasion from the river surface of the Congo basin (32 Tg C yr^{-1}) is the same as that estimated by Raymond et al. (2013) (also 32 Tg C yr^{-1}), downscaled over the same basin area, but smaller than the 59.7 Tg C yr^{-1} calculated by Lauerwald et al. (2015) and far smaller than that of Borges et al. (2015[a]), 133-177 Tg C yr^{-1} or Borges et al. (2019), 251±46 Tg C yr^{-1}. The recent study of Borges et al. (2019) is based on by far and away the most extensive dataset of Congo basin pCO_2 measurements to date and thus suggests that we substantially underestimate total riverine CO_2 evasion. As previously discussed, we simulate the broad spatial and temporal variation in observed DOC and pCO_2 (2015[a, b], Fig. 5, Table 3) relatively well. It is therefore somewhat surprising that our basin-wide estimate of riverine CO_2 evasion is so different. Below we discuss some possible explanations for this discrepancy related to methodological differences and limitations.

One potential cause for the differences could be the river gas exchange velocity *k*. However, we applied a mean riverine gas exchange velocity *k* of 3.5 m d^{-1} which is similar to the 2.9 m d^{-1} used by Borges et al. (2015[a]). Moreover, a sensitivity analysis was performed in Lauerwald et al. (2017) which showed that in the physical approach of ORCHILEAK, CO_2 evasion is not very sensitive to the *k* value, unlike data-driven models. Namely, Lauerwald et al (2017) showed that an increase or decrease of *k600* for rivers and swamps of 50% only led to 1% and

589 -4% change in total CO_2 evasion, respectively. Therefore, we can discount *k* as a major source
590 of the discrepancy.

591 Another potential reason for our smaller riverine CO_2 evasion could be river surface area. We
592 simulate a mean present day (1980-2010) total river surface area of 25,900 km^2, compared to
593 the value of 23,670 km^2 used in Borges et al (2019, supplementary information) and so
594 similarly we think that this can be discounted as a major source of discrepancy.

595 The difference in our simulated riverine CO_2 evasion compared to the empirically derived
596 estimate of Borges et al. (2019), could be caused by the lack of representation of aquatic plants
597 in the ORCHILEAK model. Borges et al. (2019) used the stable isotope composition of δ^{13} C-
598 DIC to determine the origin of dissolved CO_2 in the Congo River system and found that the
599 values were consistent with a DIC input from the degradation of organic matter, in particular
600 from C_4 plants. Crucially, they further found that the δ^{13} C-DIC values were unrelated to the
601 contribution of *terra-firme* C_4 plants, rather that they were more consistent with the degradation
602 of aquatic C_4 plants, namely macrophytes. ORCHILEAK does not represent aquatic plants, and
603 the wider LSM ORCHIDEE does not have an aquatic macrophyte PFT either (though root
604 respiration of floodplain plants for the PFTs represented, is accounted for as a C source). This
605 could at the very least partly explain our conservative estimate of river CO_2 evasion, given that
606 tropical macrophytes have relatively elevated NPPs. Rates as high as 3,500 g C m^{-2} yr^{-1} have
607 been measured on floodplains in the Amazon (Silva et al., 2009). While this value is higher
608 than the values simulated in the Cuvette Centrale by ORCHILEAK (Figure 8), they are of the
609 same order of magnitude and so this alone cannot fully explain the discrepancy compared to
610 the results of Borges et al. (2019). In the Amazon basin it has been shown that wetlands export
611 approximately half of their gross primary production (GPP) to the river network compared to
612 upland (*terra-firme*) ecosystems which only export a few percent (Abril et al. 2013). More
613 importantly, Abril et al. (2013) found that tropical aquatic macrophytes export 80% of their

GPP compared to just 36% for flooded forest. Therefore, the lack of a bespoke macrophyte PFT is indeed likely to be one reason for the discrepancy between our results and those of Borges, but largely due to their particularly high export efficiency to the river-floodplain network as opposed to differences in NPP. While being a significant limitation, creating and incorporating a macrophyte PFT would be a substantial undertaking given that the authors are unaware of any published dataset which has systematically mapped their distribution and abundance. It is important to note that while ORCHILEAK does not include the export of C from aquatic macrophytes it also neglects their NPP. Moreover, most aquatic macrophytes described in the literature have short (<1 year) life-cycles (Mitchel & Rogers, 1985). As such, while this model limitation is likely one of the causes for our relatively low estimate of riverine CO_2 evasion, it will only have a limited net effect on our estimate of the overall annual C balance (NBP, NEP) of the Congo basin.

Finally, another cause for the difference in riverine CO_2 evasion could be that the resolution of ORCHILEAK (0.5 degree river network and 1° for C fluxes) is not sufficient to fully capture the dynamics of the smallest streams of the Congo Basin which have been shown to have the highest DOC and CO_2 concentrations (Borges et al., 2019). Indeed, ORCHILEAK typically does not simulate the highest observed pCO_2 measurements of the smallest tributaries (i.e. > 16,000 ppm). This is partly because for the fast reservoir (headwaters) in ORCHILEAK we assume full pCO_2 equilibrium with the atmosphere over one full day, which prevents very high pCO_2 values from building in the water column.

Despite these limitations, it is important to note that in our simulations, the evasion flux from rivers only contributes 15% of total aquatic CO_2 evasion, and including the flux from wetlands/floodplains, we produce a total of 235 Tg C yr^{-1}. Moreover, the majority of this evasion occurs in the Cuvette Centrale (Fig. 8) which suggests that while ORHILEAK fails to attribute a large portion of this flux to small rivers (owing to the coarse resolution of the river

network) we nonetheless do capture the source of carbon. In other words, in ORCHILEAK the majority of this carbon evades directly from the floodplain and wetlands of the Cuvette Centrale as opposed to the small rivers.

Our simulated export of C to the coast of 15 (15.3) Tg C yr^{-1} is virtually identical to the TOC+DIC export estimated by Borges et al. (2015[a]) of 15.5 Tg C yr^{-1}, which is consistent with the fact that we simulate a similar spatial variation of DOC concentrations (Fig. 8 and Fig. 1 for locations). It is also relatively similar to the 19 Tg C yr^{-1} (DOC + DIC) estimated by Valentini et al. (2014) in their synthesis of the African carbon budget. Valentini et al. (2014) used the largely empirical based Global Nutrient Export from WaterSheds (NEWS) model framework and they point out that Africa was underrepresented in the training data used to develop the regression relationships which underpin the model, and thus this could explain the small disagreement.

Of the total 15 Tg C yr^{-1} exported to the coast, we simulate a 2.4 Tg C yr^{-1} component of dissolved CO_2, which is relatively similar to the empirically derived estimate of the total DIC export of 3.3 Tg C yr^{-1} calculated in Wang et al. (2013). According to Wang et al., dissolved CO_2 accounts for the majority (1.9 Tg C yr^{-1}) with the rest being the weathering derived flux of HCO_3^-. Thus, the discrepancy between the two estimates is likely to be largely caused by our lack of accounting for the weathering derived flux (HCO_3^-) which they estimate at 1.4 Tg C yr^{-1}. In summary, despite this model limitation the results of Wang et al. (2013) suggest that we still capture the majority of the DIC flux.

4.2 Trends in terrestrial and aquatic carbon fluxes

There is relatively sparse observed data available on the long-term trends of terrestrial C fluxes in the Congo. Yin et al. (2017) used MODIS data to estimate NPP between 2001 and 2013

across central Africa. They found that NPP increased on average by 10 g C m^{-2} per year, while we simulate an average annual increase of 4 g C m^{-2} yr^{-1} over the same period across the Congo Basin. The two values are not directly comparable as they do not cover precisely the same geographic area but it is encouraging that our simulations exhibit a similar trend to remote sensing data. As previously noted, MODIS derived estimates of NPP do not fully include the effect of CO_2 fertilization (de Kauwe et al., 2016) whereas ORCHILEAK does. Thus, the MODIS NPP product may underestimate the increasing trend in NPP, which would bring our modeled trend further away from this dataset. On the other hand, forest degradation effects and recent droughts have been associated with a decrease of greenness (Zhou et al., 2014) and above ground biomass loss (Qie et al., 2019) in tropical forests.

Up to a point, our results also concur with estimates based on the upscaling of biomass observations (Lewis et al., 2009; Hubau et al., 2019). Lewis et al. (2009) up-scaled forest plot measurements to calculate that intact tropical African forests represented a net uptake of approximately 300 Tg C yr^{-1} between 1968 and 2007 and this is consistent with our NEP estimate of 275 Tg C yr^{-1} over the same period. However, more recently an analysis based on an extension of the same dataset found that the above ground C sink in tropical Africa was relatively stable from 1985 to 2015 (Hubau et al., 2020).

A major source of the uncertainty associated with future projections of NPP and NEP comes from our limited understanding and representation of the CO_2 fertilization effect. Recent analysis of data from some of the longest-running Free-Air CO_2 Enrichment (FACE) sites, consisting of early-successional temperate ecosystems, found a $29.1 \pm 11.7\%$ stimulation of biomass over a decade (Walker et al., 2019). A meta-analysis (Liu et al., 2019) of seven temperate FACE experiments combined with process-based modelling also found substantial sensitivity (0.64 ± 0.28 PgC yr^{-1} per hundred ppm) of biomass accumulation to atmospheric CO_2 increase, and the same study showed that ORCHIDEE model simulations were largely

688 consistent with the experiments. However, other FACE experiments on mature temperate
689 forests (Körner et al., 2005), as well as eucalyptus forests bring into question whether the
690 fertilization effects observed in temperate FACE experiments can be extrapolated to other
691 ecosystems. For example, the Swiss FACE study, a deciduous mature forest, found no
692 significant biomass increase with enhanced CO_2 (Körner et al., 2005), while a FACE
693 experiment on a mature eucalyptus forest in Australia found that while CO_2 stimulated an
694 increase in C uptake through GPP, this did not carry to the ecosystem level, largely as a result
695 of a concurrent increase in soil respiration (Jiang et al., 2020). Unfortunately, no results are yet
696 available from any tropical FACE experiments, though the Amazon FACE experiment is
697 underway and the eventual results will be crucial in developing our understanding of the CO_2
698 fertilization effect beyond the temperate zone.

699 With these limitations in our understanding of tropical forest ecosystems in mind, over the
700 entire simulation period (1861-2099) we estimate that aquatic CO_2 evasion will increase by
701 79% and the export of C to the coast by 67%. This increase is considerably higher than the
702 23% and 27% rise in outgassing and export predicted for the Amazon basin (Lauerwald et al.,
703 2020), over the same period and under the same scenario. This is largely due to the fact climate
704 change is predicted to have a substantial negative impact on the aquatic C fluxes in the Amazon,
705 something that we do not find for the Congo where rainfall is projected to substantially increase
706 over the 21st century (RCP 6.0). In the Amazon, Lauerwald et al. (2020) show that while there
707 are decadal fluctuations in precipitation and discharge, total values across the basin remain
708 unchanged in 2099 compared to 1861. However, changes in the spatial distribution of
709 precipitation mean that the total water surface area actually decreases in the Amazon. Indeed,
710 while we find an increase in the ratio of C exports to the LOAC/NPP from 3 to 5%, Lauerwald
711 et al. (2020) find a comparative decrease.

712 Our simulated increase in DOC export to the coast up to the present day is smaller than findings
713 recently published for the Mississippi River using the Dynamic Land Ecosystem Model
714 (DLEM, Ren at al., 2016). In addition, the Mississippi study identified LUC including land
715 management practices (e.g. irrigation and fertilization), followed by change in atmospheric
716 CO_2, as the biggest factors in the 40% increase in DOC export to the Gulf of Mexico (Ren et
717 al., 2016). Another recent study (Tian et al., 2015), found an increase in DIC export from
718 eastern North America to the Atlantic Ocean from 1901-2008 but no significant trend in DOC.
719 They demonstrated that climate change and increasing atmospheric CO_2 had a significant
720 positive effect on long-term C export while land-use change had a substantial negative impact.

721 **4.3 Limitations and further model developments**

722 It is important to note that we can have greater confidence in the historic trend (until present-
723 day), as the future changes are more reliant on the skill of Earth System model predictions and
724 of course on the accuracy of the RCP 6.0 scenario. As discussed above, our understanding and
725 representation of CO_2 fertilization, especially in the tropics, is a major limitation. Moreover,
726 the majority of land surface models, ORCHILEAK included in its current iteration, do not
727 represent the effect of nutrient limitation on plant growth meaning that estimates of land C
728 uptake may be too large (Goll et al., 2017). There are also considerable uncertainties associated
729 with future climate projections in the Congo basin (Haensler et al., 2013). Nutrient limitation
730 on growth and a better representation of effect of enhanced CO_2, particularly with regards to
731 soil respiration (Jiang et al., 2020) and tree mortality (Hubau et al., 2020), are two crucial
732 aspects which need to be further developed.

733 Additionally, we do not account for methane fluxes from Congo wetlands, estimated at 1.6 to
734 3.2 Tg (CH_4) per year (Tathy et al., 1992), and instead assume that all C is evaded in the form
735 of CO_2. Another limitation is the lack of accounting for bespoke peatland dynamics in the

ORCHILEAK model. ORCHILEAK is able to represent the general reduction in C decomposition in water-logged soils and indeed Hastie et al. (2019) demonstrated that increasing the maximum floodplain extent in the Amazon Basin led to an increase in NEP despite fueling aquatic CO_2 evasion because of the effect of reducing soil heterotrophic respiration. Furthermore, ORCHILEAK uses a "poor soils" mask forcing file (Fig. 2 j) based on the Harmonized World Soil Database (FAO/IIASA/ISRIC/ISS-CAS/JRC, 2009), which prescribes reduced decomposition rates in low nutrient and pH soils (e.g. Podzols and Arenosols). The effect of the "poor soils" forcing can clearly be seen in the spatial distribution of the soil C stock in Fig. A3, where the highest C storage coincides with the highest proportion of poor soils. Interestingly, this does not include the Cuvette Centrale wetlands (Fig. 1), an area which was recently identified as containing the world's largest intact tropical peatland and a stock of around 30 Pg C (Dargie at al., 2017). One potential improvement that could be made to ORCHILEAK would be the development of a new tailored "poor soils" forcing file for the Congo Basin which explicitly includes Histosols, perhaps informed by the Soil Grids database (Hengl et al., 2014), to better represent the Cuvette Centrale. This could in turn, be validated and/or calibrated against the observations of Dargie et al. (2017). A more long-term aim could be the integration/ coupling of the ORCHIDEE-PEAT module with ORCHILEAK. ORCHIDEE-PEAT (Qiu et al., 2019) represents peat as an independent sub-grid hydrological soil unit in which peatland soils are characterized by peat-specific hydrological properties and multi-layered transport of C and water. Thus far, it has only been applied to northern peatlands, and calibrating it to tropical peatlands, along with integrating it within ORCHILEAK would require considerable further model development, but would certainly be a valuable longer-term aspiration. This could also be applied across the tropical region and would allow us to comprehensively explore the implications of climate change and land-use change for tropical peatlands. In addition, ORCHILEAK does not simulate the erosion and subsequent burial of

761 POC within river and floodplain sediments. Although it does not represent the lateral transfer
762 of POC, it does incorporate the decomposition of inundated litter as an important source of
763 DOC and dissolved CO_2 to the aquatic system; i.e. it is assumed that POC from submerged
764 litter decomposes locally in ORCHILEAK. Moreover, previous studies have found that DOC
765 as opposed to POC (Spencer et al., 2016; Bouillon et al., 2012) overwhelmingly dominates the
766 total load of C in the Congo.

767 The representation of the rapid C loop of aquatic macrophytes should also be made a priority
768 in terms of improving models such as ORCHILEAK, particularly in the tropics. As previously
769 discussed, ORCHILEAK also fails to account for the weathering derived flux (HCO_3^-). Finally,
770 the issue of shifting cultivation demands further attention; at least for the present day a shifting
771 cultivation forcing file could be developed based on remote sensing data (Tyukavina et al.,
772 2018). For additional discussion of the limitations of ORCHILEAK, please also see Lauerwald
773 et al. (2017) and Hastie et al. (2019).

774 ## 5. Conclusions

775 For the present day, we show that aquatic C fluxes, and in particular CO_2 evasion, are important
776 components of the Congo Basin C balance, larger than for example the combined fluxes from
777 LUC and harvesting, with around 4% of terrestrial NPP being exported to the aquatic system
778 each year. Our simulations show that these fluxes may have undergone considerable
779 perturbation since 1861 to the present day, and that under RCP 6.0 this perturbation could
780 continue; over the entire simulation period (1861-2099), we estimate that aquatic CO_2 evasion
781 will increase by 79% and the export of C to the coast by 67%. We further find that the ratio of
782 C exports to the LOAC/NPP could increase from 3 to 5%, driven by both rising atmospheric
783 CO_2 concentrations and climate change. This calls for long-term monitoring of C levels and
784 fluxes in the rivers of the Congo basin, and further investigation of the potential impacts of

785 such change. Our results also highlight the limitations of the current generation of land surface
786 models and call for investment into further model development.

787

788 *Code availability*. A description of the general ORCHIDEE code can be found here:
789 http://forge.ipsl.jussieu.fr/orchidee/browser#tags/ORCHIDEE_1_9_6/ORCHIDEE.

790 The main part of the ORCHIDEE code was written by Krinner et al. (2005). See d'Orgeval et
791 al. (2008) for a general description of the river routing scheme. For the updated soil C module
792 please see Camino Serrano (2015). For the source code of ORCHILEAK see Lauerwald et al.
793 (2017)- https://doi.org/10.5194/gmd-10-3821-2017-supplement

794 For details on how to install ORCHIDEE and its various branches, please see the user guide:
795 http://forge.ipsl.jussieu.fr/orchidee/ wiki/Documentation/UserGuide

796 *Author contribution*. AH, RL, PR and PC all contributed to the conceptualization of the study.
797 RL developed the model code, AH developed the novel forcing files for Congo, and AH
798 performed the simulations. FP provided the GIEMS dataset for model validation. AH prepared
799 the manuscript with contributions from all co-authors. RL and PR provided supervision and
800 guidance to AH throughout the research. PR acquired the primary financial support that
801 supported this research.

802 *Competing interests*. The authors declare that they have no conflict of interest.

803 *Financial support*. Financial support was received from the European Union's Horizon 2020
804 research and innovation programme under the Marie Sklodowska- Curie grant agreement No.
805 643052 (C-CASCADES project). PR acknowledges funding from the European Union's
806 Horizon 2020 research and innovation programme under Grant Agreement 776810 (project
807 VERIFY). RL acknowledges funding from the ANR ISIPEDIA ERA4CS project.

References

Abril, G., Martinez, J.-M., Artigas, L. F., Moreira-Turcq, P., Benedetti, M. F., Vidal, L., … Roland, F. (2013). Amazon River carbon dioxide outgassing fuelled by wetlands. *Nature*, *505*, 395. Retrieved from http://dx.doi.org/10.1038/nature12797

Battin, T. J., Luyssaert, S., Kaplan, L. A., Aufdenkampe, A. K., Richter, A., & Tranvik, L. J. (2009). The boundless carbon cycle. *Nature Geoscience*, *2*, 598. Retrieved from https://doi.org/10.1038/ngeo618

Becker, M.; Papa, F.; Frappart, F.; Alsdorf, D.; Calmant, S.; Da Silva, J.S.; Prigent, C.; Seyler, F. Satellite-based estimates of surface water dynamics in the Congo River Basin. Int. J. Appl. Earth Obs. Geoinf. 2018, 196–209

Borges, A. V, Darchambeau, F., Teodoru, C. R., Marwick, T. R., Tamooh, F., Geeraert, N., … Bouillon, S. (2015)[a]. Globally significant greenhouse-gas emissions from African inland waters. *Nature Geoscience*, *8*, 637. Retrieved from https://doi.org/10.1038/ngeo2486

Borges, A. V, Abril, G., Darchambeau, F., Teodoru, C. R., Deborde, J., Vidal, L. O., … Bouillon, S. (2015)[b]. Divergent biophysical controls of aquatic CO2 and CH4 in the World's two largest rivers. *Scientific Reports*, *5*, 15614. https://doi.org/10.1038/srep15614

Borges, A. V., Darchambeau, F., Lambert, T., Morana, C., Allen, G. H., Tambwe, E., Toengaho Sembaito, A., Mambo, T., Nlandu Wabakhangazi, J., Descy, J.-P., Teodoru, C. R., and Bouillon, S (2019).: Variations in dissolved greenhouse gases (CO_2, CH_4, N_2O) in the Congo River network overwhelmingly driven by fluvial-wetland connectivity, Biogeosciences, 16, 3801–3834, https://doi.org/10.5194/bg-16-3801-2019.

Bouillon, S., Yambélé, A., Spencer, R. G. M., Gillikin, D. P., Hernes, P. J., Six, J., Merckx, R., and Borges, A. V.: Organic matter sources, fluxes and greenhouse gas exchange in the Oubangui River (Congo River basin), Biogeosciences, 9, 2045–2062, https://doi.org/10.5194/bg-9-2045-2012, 2012.

Bouillon, S., Yambélé, A., Gillikin, D. P., Teodoru, C., Darchambeau, F., Lambert, T., & Borges, A. V. (2014). Contrasting biogeochemical characteristics of the Oubangui River and tributaries (Congo River basin). *Scientific Reports*, *4*, 5402. Retrieved from https://doi.org/10.1038/srep05402

Bowring, S. P. K., Lauerwald, R., Guenet, B., Zhu, D., Guimberteau, M., Tootchi, A., Ducharne, A., and Ciais, P (2019)[a].: ORCHIDEE MICT-LEAK (r5459), a global model for the production, transport, and transformation of dissolved organic carbon from Arctic permafrost regions – Part 1: Rationale, model description, and simulation protocol, Geosci. Model Dev., 12, 3503–3521, https://doi.org/10.5194/gmd-12-3503-2019, 2019.

Bowring, S. P. K., Lauerwald, R., Guenet, B., Zhu, D., Guimberteau, M., Regnier, P., Tootchi, A., Ducharne, A., and Ciais, P (2019)[b].: ORCHIDEE MICT-LEAK (r5459), a global model for the production, transport and transformation of dissolved organic carbon from Arctic permafrost regions, Part 2: Model evaluation over the Lena River basin, Geosci. Model Dev. Discuss., https://doi.org/10.5194/gmd-2018-322, in review, 2019.

Camino-Serrano, M., Guenet, B., Luyssaert, S., Ciais, P., Bastrikov, V., De Vos, B., Gielen, B., Gleixner, G., Jornet-Puig, A., Kaiser, K., Kothawala, D., Lauerwald, R., Peñuelas, J., Schrumpf, M., Vicca, S., Vuichard, N., Walmsley, D., and Janssens, I. A.: ORCHIDEE-SOM: modeling soil organic carbon (SOC) and dissolved organic carbon (DOC) dynamics along vertical soil profiles in Europe, Geosci. Model Dev., 11, 937–957, https://doi.org/10.5194/gmd-11-937-2018, 2018

CBFP (Congo Basin Forest Partnership) (2009). The forests of the Congo Basin — State of the Forest 2008, Publications Office of the European Union, Luxembourg (2009), 10.2788/32259

Ciais, P., Piao, S.-L., Cadule, P., Friedlingstein, P., & Chédin, A. (2009). Variability and recent trends in the African terrestrial carbon balance. *Biogeosciences*, *6*(9), 1935–1948. https://doi.org/10.5194/bg-6-1935-2009

Ciais, P., Yao, Y., Gasser, T., Baccini, A., Wang, Y., Lauerwald, R., … Zhu, D. (2020). Empirical estimates of regional carbon budgets imply reduced global soil heterotrophic respiration. *National Science Review*. https://doi.org/10.1093/nsr/nwaa145

Cochonneau, G., Sondag, F., Guyot, J.-L., Geraldo, B., Filizola, N., Fraizy, P., Laraque, A., Magat, P., Martinez, J.-M., Nor iega, L., Oliveira, E., Ordonez, J., Pombosa, R., Seyler, F., Sidgwick, J., and Vauchel, P.: The environmental observation and research project, ORE HYBAM, and the rivers of the Amazon basin, in: Climate Variability and Change – Hydrological Impacts, IAHS Publ. 308, edited by: Demuth, S., Gustard, A., Planos, E., Scatena, F., and Servat, E., IAHS Press, UK, 44–50, 2006

Coynel, A., P. Seyler, H. Etcheber, M. Meybeck, and D. Orange (2005), Spatial and seasonal dynamics of total suspended sediment and organic carbon species in the Congo River, *Global Biogeochem. Cycles*, 19, GB4019, doi:10.1029/2004GB002335.

Creese, A., Washington, R., & Jones, R. (2019). Climate change in the Congo Basin: processes related to wetting in the December–February dry season. *Climate Dynamics*, *53*(5), 3583–3602. https://doi.org/10.1007/s00382-019-04728-x

Dargie, G. C., Lewis, S. L., Lawson, I. T., Mitchard, E. T. A., Page, S. E., Bocko, Y. E., & Ifo, S. A. (2017). Age, extent and carbon storage of the central Congo Basin peatland complex. *Nature*, *542*, 86. Retrieved from https://doi.org/10.1038/nature21048

De Kauwe, M. G., Keenan, T. F., Medlyn, B. E., Prentice, I. C. and Terrer. C. (2016) Satellite based estimates underestimate the effect of CO_2 fertilisation on net primary productivity. *Nature Climate Change*, 6, 892-893

d'Orgeval, T., Polcher, J., & de Rosnay, P. (2008). Sensitivity of the West African hydrological cycle in ORCHIDEE to infiltration processes. *Hydrology and Earth System Sciences*, **12**, 1387– 1401. https://doi.org/10.5194/hess-12-1387-2008

Drake, T. W., Raymond, P. A., & Spencer, R. G. M. (2018). Terrestrial carbon inputs to inland waters: A current synthesis of estimates and uncertainty. Limnology and Oceanography Letters, 3(3), 132–142. http://doi.org/10.1002/lol2.10055

Fan, L., Wigneron, J.-P., Ciais, P., Chave, J., Brandt, M., Fensholt, R., … Peñuelas, J. (2019). Satellite-observed pantropical carbon dynamics. *Nature Plants*, *5*(9), 944–951. https://doi.org/10.1038/s41477-019-0478-9

FAO/IIASA/ISRIC/ISS-CAS/JRC: Harmonized World Soil Database (version 1.1), FAO, Rome, 2009.

Fisher JB, Sikka M, Sitch S, Ciais P, Poulter B, Galbraith D, Lee J-E, Huntingford C, Viovy N, Zeng N, Ahlstro¨m A, Lomas MR, Levy PE, Frankenberg C, Saatchi S, Malhi Y. 2013 African tropical rainforest net carbon dioxide fluxes in the twentieth century. Phil Trans R Soc B 368: 20120376.http://dx.doi.org/10.1098/rstb.2012.0376

Frieler, K., Lange, S., Piontek, F., Reyer, C. P. O., Schewe, J., Warszawski, L., … Yamagata, Y. (2017). Assessing the impacts of 1.5 °C global warming – simulation protocol of the Inter-Sectoral Impact Model Intercomparison Project (ISIMIP2b). *Geosci. Model Dev.*, *10*(12), 4321–4345. https://doi.org/10.5194/gmd-10-4321-2017

Goll, D. S., Vuichard, N., Maignan, F., Jornet-Puig, A., Sardans, J., Violette, A., Peng, S., Sun, Y., Kvakic, M., Guimberteau, M., Guenet, B., Zaehle, S., Penuelas, J., Janssens, I., and Ciais, P.: A representation of the phosphorus cycle for ORCHIDEE (revision 4520), Geosci. Model Dev., 10, 3745-3770, https://doi.org/10.5194/gmd-10-3745-2017, 2017.

Guimberteau, M., Drapeau, G., Ronchail, J., Sultan, B., Polcher, J., Martinez, J.-M., Prigent, C., Guyot, J.-L., Cochonneau, G., Espinoza, J. C., Filizola, N., Fraizy, P., Lavado, W., De Oliveira, E., Pombosa, R., Noriega, L., and Vauchel, P.: Discharge simulation in the sub-basins of the Amazon using ORCHIDEE forced by new datasets, Hydrol. Earth Syst. Sci., 16, 911–935, https://doi.org/10.5194/hess-16-911-2012, 2012.

Gumbricht, T., Roman-Cuesta, R. M., Verchot, L., Herold, M., Wittmann, F., Householder, E., Murdiyarso, D. (2017). An expert system model for mapping tropical wetlands and peatlands reveals South America as the largest contributor. *Global Change Biology*, *23*(9), 3581–3599. https://doi.org/10.1111/gcb.13689

Haensler, A., Saeed, F. and Jacob, D. (2013): Assessment of projected climate change signals over central Africa based on a multitude of global and regional climate projections. In: Climate Change Scenarios for the Congo Basin. [Haensler A., Jacob D., Kabat P., Ludwig F. (eds.)]. Climate Service Centre Report No. 11, Hamburg, Germany, ISSN: 2192-4058

Hastie, A., Lauerwald, R., Ciais, P., Regnier, P (2019). Aquatic carbon fluxes dampen the overall variation of net ecosystem productivity in the Amazon basin: An analysis of the interannual variability in the boundless carbon cycle**.** *Global Change Biology*,; 25: 2094– 2111. https://doi.org/10.1111/gcb.14620

Hartmann, J., R. Lauerwald, and N. Moosdorf (2014), A brief overview of the GLObal RIver CHemistry Database, GLORICH, Procedia Earth Planet. Sci., **10**, 23–27.

Heinimann A, Mertz O, Frolking S, Egelund Christensen A, Hurni K, Sedano F, et al. (2017) A global view of shifting cultivation: Recent, current, and future extent. PLoS ONE 12(9): e0184479. https://doi.org/10.1371/journal.pone.0184479

926 Hengl, T., de Jesus, J. M., MacMillan, R. A., Batjes, N. H., Heuvelink, G. B. M., Ribeiro, E.,
927 … Ruiperez Gonzalez, M. (2014). SoilGrids1km-global soil information based on automated
928 mapping. PLoS One, 9, e105992. https://doi.org/10.1371/journal.pone.0105992

929 Hubau, W.; Lewis, S.L.; Phillips, O.L.; Affum-Baffoe, K.; Beeckman, H.; Cuní-Sanchez, A.;
930 Daniels, A.K.; Ewango, C.E.N.; Fauset, S.; Mukinzi, J.M.; et al. Asynchronous carbon sink
931 saturation in African and Amazonian tropical forests. Nature 2020, 579, 80–87.

932 Hurtt, G. C., Chini, L. P., Frolking, S., Betts, R. A., Feddema, J., Fischer, G., … Wang, Y. P.
933 (2011). Harmonization of land-use scenarios for the period 1500--2100: 600 years of global
934 gridded annual land-use transitions, wood harvest, and resulting secondary lands. *Climatic*
935 *Change*, *109*(1), 117. https://doi.org/10.1007/s10584-011-0153-2

936 Jiang, M., Medlyn, B.E., Drake, J.E. *et al.* The fate of carbon in a mature forest under carbon
937 dioxide enrichment. *Nature* **580,** 227–231 (2020). https://doi.org/10.1038/s41586-020-2128-9

938 Kim, H. (2017). *Global Soil Wetness Project Phase 3 Atmospheric Boundary Conditions*
939 *(Experiment 1)* [Data set]. Data Integration and Analysis System (DIAS).
940 https://doi.org/10.20783/DIAS.501

941 Korner C, Asshoff R, Bignucolo O (2005) Carbon flux and growth in mature deciduous forest
942 trees exposed to elevated CO2. Science, 309, 1360–1362.

943 Lange., S (2017). "ISIMIP2b Bias-Correction Code," ***Zenodo***, doi: 10.5281/zenodo.1069050

944 Laudon, H., and I. Buffam (2008), Impact of changing DOC concentrations on the potential
945 distribution of acid sensitive biota in a boreal stream network, *Hydrol. Earth Syst.*
946 *Sci.*, **12**(2), 425–435.

947 Lauerwald, R., Laruelle, G. G., Hartmann, J., Ciais, P., & Regnier, P. A. G. (2015). Spatial
948 patterns in CO2 evasion from the global river network. *Global Biogeochemical Cycles*, *29*(5),
949 534–554. https://doi.org/10.1002/2014GB004941

950 Lauerwald, R., Regnier, P., Camino-Serrano, M., Guenet, B., Guimberteau, M., Ducharne,
951 A., … Ciais, P. (2017). ORCHILEAK (revision 3875): a new model branch to simulate
952 carbon transfers along the terrestrial--aquatic continuum of the Amazon basin. *Geoscientific*
953 *Model Development*, *10*(10), 3821–3859. https://doi.org/10.5194/gmd-10-3In821-2017

954 Lauerwald, R., Regnier, P., Guenet, B., Friedlingstein, P; Ciais, P (2020): How simulations of
955 the land carbon sink are biased by ignoring fluvial carbon transfers – A case study for the
956 Amazon basin. *One Earth*, 10.1016/j.oneear.2020.07.009.

957 Lee, H., Beighley, R. E., Alsdorf, D., Jung, H. C., Shum, C. K., Duan, J., … Andreadis, K.
958 (2011). Characterization of terrestrial water dynamics in the Congo Basin using GRACE and
959 satellite radar altimetry. *Remote Sensing of Environment*, *115*(12), 3530–3538.
960 https://doi.org/https://doi.org/10.1016/j.rse.2011.08.015

961 Lehner, B., & Döll, P. (2004). Development and validation of a global database of lakes,
962 reservoirs and wetlands. *Journal of Hydrology*, *296*(1–4), 1–22.
963 https://doi.org/https://doi.org/10.1016/j.jhydrol.2004.03.028

964 Lewis, S. L., Lopez-Gonzalez, G., Sonké, B., Affum-Baffoe, K., Baker, T. R., Ojo, L. O., …
965 Wöll, H. (2009). Increasing carbon storage in intact African tropical forests. *Nature*, *457*,
966 1003. Retrieved from https://doi.org/10.1038/nature07771

967 Liu, Y., Piao, S., Gasser, T., Ciais, P., Yang, H., Wang, H., … Wang, T. (2019). Field-
968 experiment constraints on the enhancement of the terrestrial carbon sink by CO2 fertilization.
969 Nature Geoscience, 12(10), 809–814. https://doi.org/10.1038/s41561-019-0436-1

970 Masui, T., Matsumoto, K., Hijioka, Y., Kinoshita, T., Nozawa, T., Ishiwatari, S., Kato, E.,
971 Shukla, P.R., Yamagata, Y., Kainuma, M., 2011. A emission pathway to stabilize at 6 W/m2
972 of radiative forcing, Climatic Change, doi:10.1007/s10584-011-0150-5. Morgan, M.G.,
973 Adams, P., Keith, D.W., 2006. Elicitation of expert judgments of aerosol forcing. Climatic
974 Change 75, 195–214

975 Melack, J.M., Hess, L.L., Gastil, M., Forsberg, B.R., Hamilton, S.K., Lima, I.B. and Novo,
976 E.M. (2004), Regionalization of methane emissions in the Amazon Basin with microwave
977 remote sensing. Global Change Biology, 10: 530-544. doi:10.1111/j.1365-2486.2004.00763.x

978 Mitchell D.S., Rogers K.H. (1985) Seasonality/aseasonality of aquatic macrophytes in
979 Southern Hemisphere inland water. In: Davies B.R., Walmsley R.D. (eds) Perspectives in
980 Southern Hemisphere Limnology. Developments in Hydrobiology, vol 28. Springer,
981 Dordrecht

982 Nash, J. E., and J. V. Sutcliffe. 1970. River flow forecasting through conceptual models: Part
983 1. A discussion of principles. J. Hydrology 10(3): 282-290

984 O'Loughlin, F., M. A. Trigg, G. J.-P. Schumann, and P. D. Bates (2013), Hydraulic
985 characterization of the middle reach of the Congo River, *Water Resour. Res.*, 49, 5059–5070,
986 doi:10.1002/wrcr.20398.

987 Pan, S., Dangal, S. R. S., Tao, B., Yang, J., & Tian, H. (2015). Recent patterns of terrestrial
988 net primary production in Africa influenced by multiple environmental changes. *Ecosystem*
989 *Health and Sustainability*, *1*(5), 1–15. https://doi.org/10.1890/EHS14-0027.1

990 Papa, F., Prigent, C., Aires, F., Jimenez, C., Rossow, W. B., and Matthews,
991 E. (2010), Interannual variability of surface water extent at the global scale, 1993–2004, *J.*
992 *Geophys. Res.*, 115, D12111, doi:10.1029/2009JD012674.

993 Potapov, P. V, Turubanova, S. A., Hansen, M. C., Adusei, B., Broich, M., Altstatt, A., …
994 Justice, C. O. (2012). Quantifying forest cover loss in Democratic Republic of the Congo,
995 2000–2010, with Landsat ETM+ data. *Remote Sensing of Environment*, *122*, 106–116.
996 https://doi.org/https://doi.org/10.1016/j.rse.2011.08.027

997 Potter, C., Klooster, S., & Genovese, V. (2012). Net primary production of terrestrial
998 ecosystems from 2000 to 2009. *Climatic Change*, *115*(2), 365–378.
999 https://doi.org/10.1007/s10584-012-0460-2

1000 Prigent, C., Papa, F., Aires, F., Rossow, W. B., and Matthews, E.: Global inundation
1001 dynamics inferred from multiple satellite observations, 1993–2000, J. Geophys. Res., 112,
1002 D12107, https://doi.org/10.1029/2006jd007847, 2007.

Qie, L., Telford, E. M., Massam, M. R., Tangki, H., Nilus, R., Hector, A., & Ewers, R. M. (2019). Drought cuts back regeneration in logged tropical forests. *Environmental Research Letters*, *14*(4), 45012. https://doi.org/10.1088/1748-9326/ab0783

Qiu, C., Zhu, D., Ciais, P., Guenet, B., Peng, S., Krinner, G., Tootchi, A., Ducharne, A., and Hastie, A.: Modelling northern peatland area and carbon dynamics since the Holocene with the ORCHIDEE-PEAT land surface model (SVN r5488), Geosci. Model Dev., 12, 2961–2982, https://doi.org/10.5194/gmd-12-2961-2019, 2019.

R Core Team. (2013). R: A language and environment for statistical computing. [Available at http://www.r-project.org.]

Raymond, P. A., Hartmann, J., Lauerwald, R., Sobek, S., McDonald, C., Hoover, M., . . . Guth, P. (2013). Global carbon dioxide emissions from inland waters. Nature, 503(7476), 355–359. Retrieved from https://doi.org/10.1038/nature12760

Regnier, P., Friedlingstein, P., Ciais, P., Mackenzie, F. T., Gruber, N., Janssens, I. A., … Thullner, M. (2013). Anthropogenic perturbation of the carbon fluxes from land to ocean. *Nature Geosci*, *6*(8), 597–607. Retrieved from http://dx.doi.org/10.1038/ngeo1830

Ren, W., H. Tian, W.-J. Cai, S. E. Lohrenz, C. S. Hopkinson, W.-J. Huang, J. Yang, B. Tao, S. Pan, and R. He (2016), Century long increasing trend and variability of dissolved organic carbon export from the Mississippi River basin driven by natural and anthropogenic forcing, Global Biogeochem. Cycles, 30, 1288–1299, doi:10.1002/ 2016GB005395.

Reynolds, C., Jackson, T. & Rawls, W. Estimating available water content by linking 424 the FAO soil map of the world with global soil profile databases and pedo-transfer 425 functions. Am. Geophys. Union Fall Meet. EOS Trans. Spring Meet. Suppl. 80, S132 426 (1999).

Richey, J. E., Melack, J. M., Aufdenkampe, A. K., Ballester, V. M., & Hess, L. L. (2002). Outgassing from Amazonian rivers and wetlands as a large tropical source of atmospheric CO2. Nature, 416(6881), 617– 620. https://doi.org/10.1038/416617a

Schimel D, Stephens BB, Fisher JB. 2015.Effect of increasing CO2 on the terrestrial carbon cycle. Proceedings of the National Academy of Sciences, USA 112: 436–441

Sheffield, J., Goteti, G., & Wood, E. F. (2006). Development of a 50-Year High-Resolution Global Dataset of Meteorological Forcings for Land Surface Modeling. *Journal of Climate*, *19*(13), 3088–3111. https://doi.org/10.1175/JCLI3790.1

Silva, T.S.F., Costa, M.P.F. & Melack, J.M. Annual net primary production of macrophytes in the eastern Amazon floodplain. Wetlands (2009) 29: 747. https://doi.org/10.1672/08-107.1

Smith, W.K., Fox, A.M., MacBean, N., Moore, D.J.P. and Parazoo, N.C. (2020), Constraining estimates of terrestrial carbon uptake: new opportunities using long-term satellite observations and data assimilation. New Phytol, 225: 105-112. doi:10.1111/nph.16055

Spencer, R. G. M., P. J. Hernes, B. Dinga, J. N. Wabakanghanzi, T. W. Drake, and J. Six (2016), Origins, seasonality, and fluxes of organic matter in the Congo River, *Global Biogeochem. Cycles*, 30, 1105–1121, doi: 10.1002/2016GB005427.

Sullivan, M. J. P., Talbot, J., Lewis, S. L., Phillips, O. L., Qie, L., Begne, S. K., … Zemagho, L. (2017). Diversity and carbon storage across the tropical forest biome. *Scientific Reports*, *7*, 39102. Retrieved from https://doi.org/10.1038/srep39102

Tathy, J. P., B. Cros, R. A. Delmas, A. Marenco, J. Servant, and M. Labat (1992), Methane emission from flooded forest in central Africa, *J. Geophys. Res.*, 97(D6), 6159–6168, doi:10.1029/90JD02555.

Tian, H., Q. Yang, R. G. Najjar, W. Ren, M. A. M. Friedrichs, C. S. Hopkinson, and S. Pan (2015), Anthropogenic and climatic influences on carbon fluxes from eastern North America to the Atlantic Ocean: A process-based modeling study, J. Geophys. Res. Biogeosci., 120, 752–772, doi:10.1002/2014JG002760.

Tyukavina, A., Hansen, M. C., Potapov, P., Parker, D., Okpa, C., Stehman, S. V, … Turubanova, S. (2018). Congo Basin forest loss dominated by increasing smallholder clearing. *Science Advances*, *4*(11). https://doi.org/10.1126/sciadv.aat2993

Valentini, R., Arneth, A., Bombelli, A., Castaldi, S., Cazzolla Gatti, R., Chevallier, F., Ciais, P., Grieco, E., Hartmann, J., Henry, M., Houghton, R. A., Jung, M., Kutsch, W. L., Malhi, Y., Mayorga, E., Merbold, L., Murray-Tortarolo, G., Papale, D., Peylin, P., Poulter, B., Raymond, P. A., Santini, M., Sitch, S., Vaglio Laurin, G., van der Werf, G. R., Williams, C. A., and Scholes, R. J.: A full greenhouse gases budget of Africa: synthesis, uncertainties, and vulnerabilities, Biogeosciences, 11, 381–407, doi:10.5194/bg11-381-2014, 2014

Verhegghen, A., Mayaux, P., de Wasseige, C., & Defourny, P. (2012). Mapping Congo Basin vegetation types from 300 m and 1 km multi-sensor time series for carbon stocks and forest areas estimation. *Biogeosciences*, *9*(12), 5061–5079. https://doi.org/10.5194/bg-9-5061-2012

Viovy, N.. (2018). *CRUNCEP Version 7 - Atmospheric Forcing Data for the Community Land Model*. Research Data Archive at the National Center for Atmospheric Research, Computational and Information Systems Laboratory. http://rda.ucar.edu/datasets/ds314.3/

Walker AP, De Kauwe MG, Medlyn BE, Zaehle S, Iversen CM, Asao S, Guenet B, Harper A, Hickler T, Hungate BA et al. 2019. Decadal biomass increment in early secondary succession woody ecosystems is increased by CO2 enrichment. Nature Communications 10: 454

Weiss, L. C., Pötter, L., Steiger, A., Kruppert, S., Frost, U., & Tollrian, R. (2018). Rising pCO2 in Freshwater Ecosystems Has the Potential to Negatively Affect Predator-Induced Defenses in Daphnia. *Current Biology*, *28*(2), 327–332.e3. https://doi.org/https://doi.org/10.1016/j.cub.2017.12.022

Williams, C. A., Hanan, N. P., Neff, J. C., Scholes, R. J., Berry, J. A., Denning, A. S., and Baker, D. A.: Africa and the global carbon cycle, Carbon Balance and Management, 2(3), doi:10.1186/1750-0680-2-3, 2007.

Yin, S., Li, X., & Wu, W. (2017). Comparative analysis of NPP changes in global tropical forests from 2001 to 2013. *IOP Conference Series: Earth and Environmental Science*, *57*(1), 12009. Retrieved from http://stacks.iop.org/1755-1315/57/i=1/a=012009

Zhou, L., Tian, Y., Myneni, R. B., Ciais, P., Saatchi, S., Liu, Y. Y., … Hwang, T. (2014). Widespread decline of Congo rainforest greenness in the past decade. *Nature*, *509*(7498), 86–90. https://doi.org/10.1038/nature13265

Zhuravleva, I., Turubanova, S., Potapov, P., Hansen, M., Tyukavina, A., Minnemeyer, S., … Thies, C. (2013). Satellite-based primary forest degradation assessment in the Democratic Republic of the Congo, 2000-2010. *Environmental Research Letters*, *8*(2), 24034. https://doi.org/10.1088/1748-9326/8/2/024034

Appendix A

Table A 1: Performance statistics for modelled versus observed seasonality of discharge on the Congo at Brazzaville

Climate forcing	RSME	NSE	R^2	Mean monthly discharge ($m^3 s^{-1}$)
ISIMIP	29%	0.20	0.23	38,944
Princeton GPCC	40%	-0.25	0.20	49,784
GSWP3	46%	-4.13	0.04	24,880
CRUNCEP	65%	-15.94	0.01	16,394
Observed (HYBAM)				40,080

Table A 2: Pearson correlation coefficient (r) between detrended carbon fluxes and detrended climate variables

	SHR	Aquatic CO_2 evasion	Lateral C	NEP	Rain	Temp.	MEI
NPP	-0.48	0.68	0.72	0.90	0.64	-0.57	-0.09
SHR		-0.41	-0.48	-0.71	-0.32	0.76	0.04
Aquatic CO_2 evasion			0.92	0.41	0.87	-0.30	-0.21
Lateral C				0.52	0.81	-0.38	-0.15
NEP					0.40	-0.74	-0.01
Rain						-0.31	-0.26
Temp.							0.03

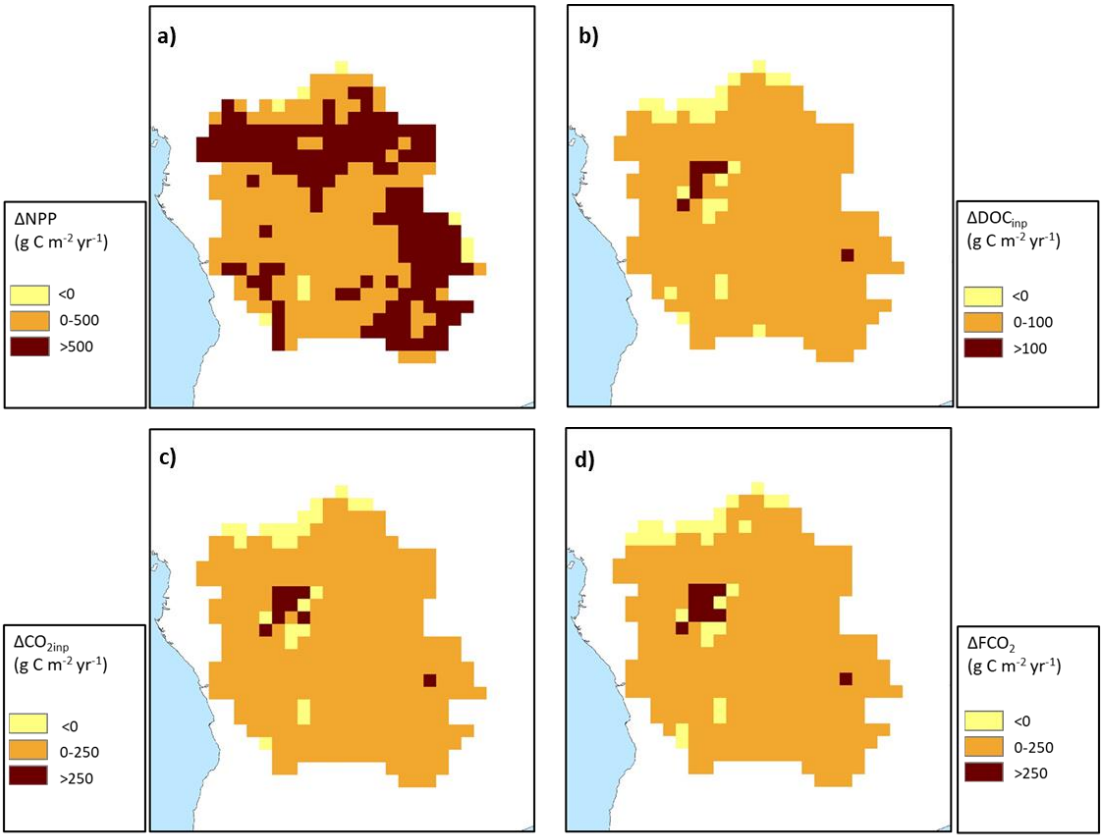

Figure A 1:Change (Δ, 2099 minus 1861) in the spatial distribution of a) terrestrial NPP, b) DOC leaching into the aquatic system, c) CO_2 leaching into the aquatic system and d) aquatic CO_2 evasion. All at a resolution of 1°

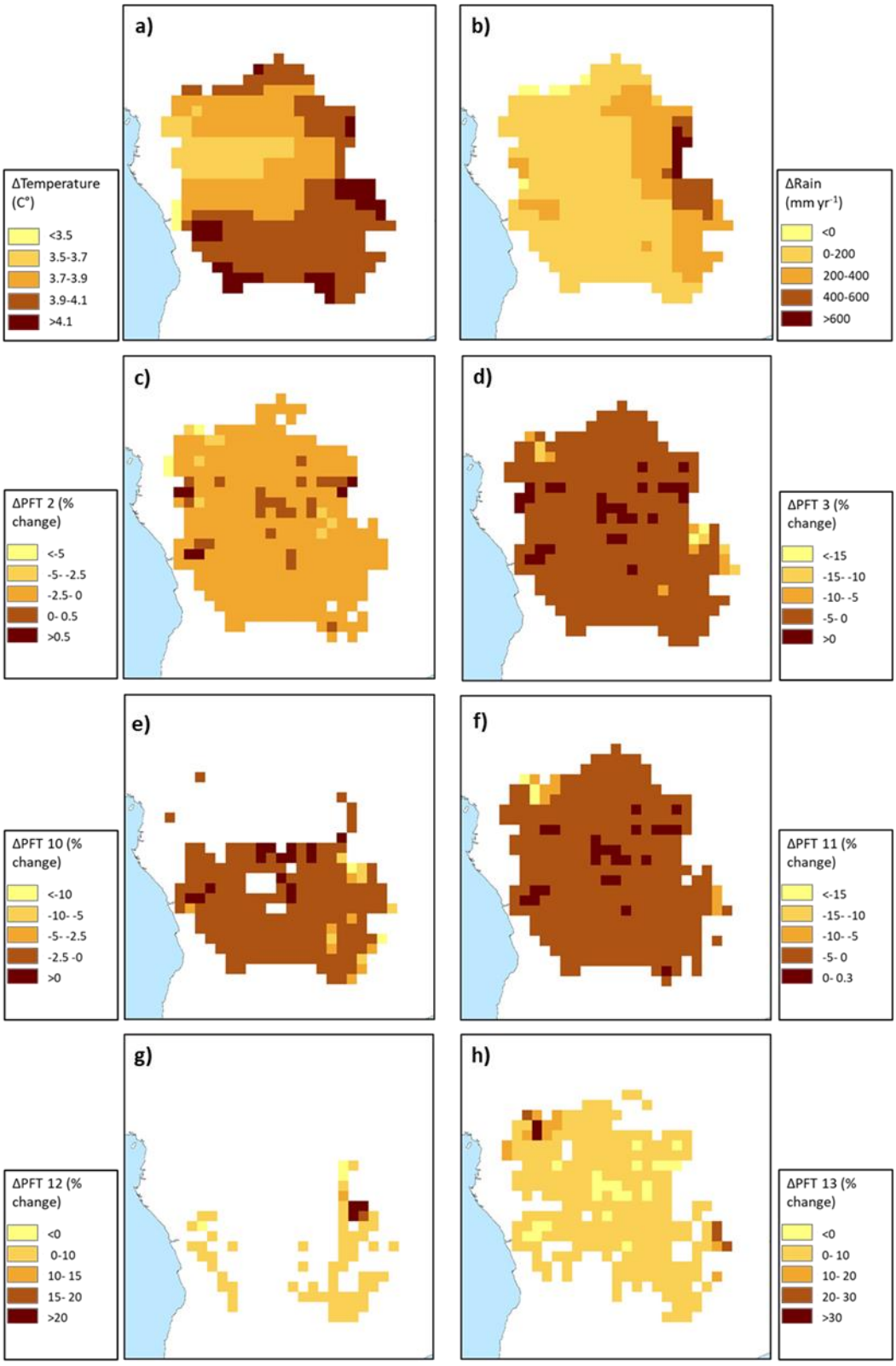

Figure A 2: Change (Δ, 2099 minus 1861) in the spatial distribution of the principal climate and land-use drivers across the Congo Basin; a) mean annual temperature in °C, b) mean annual rainfall in mm yr^{-1}, c)-h) mean annual maximum vegetated fraction for PFTs 2,3, 10,11,12 and 13. All at a resolution of 1°.

1105

1106

1107

Table A 3: Past (1861-1890), present-day (1981-2010) and future (2070-2099) mean values for important climate and land-use drivers across the Congo basin								
Period	Temp.	Rain.	PFT2	PFT3	PFT10	PFT11	PFT12	PFT13
1861-1890	24.0	1451	0.263	0.375	0.154	0.254	0.015	0.014
1981-2010	25.2	1526	0.255	0.359	0.154	0.255	0.038	0.030
2070-2099	28.2	1654	0.258	0.362	0.147	0.245	0.039	0.037

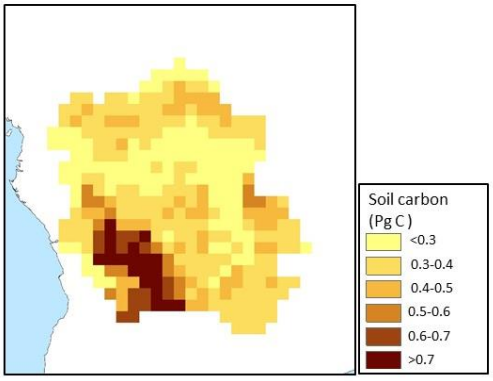

Figure A 3: Spatial distribution of simulated total carbon stored in soils for the present day (1981-2020).

1108

1109

1110